JOURNAL OF GEOPHYSICAL RESEARCH, VOL. 87, NO. B13, PAGES 10,709-10,728, DECEMBER 10, 1982

NUMERICAL MODELING OF INTRAPLATE DEFORMATION: SIMPLE MECHANICAL MODELS OF CONTINENTAL COLLISION

J. P. Vilotte and M. Daignières

Centre Géologique et Géophysique, Université des Sciences et Techniques du Languedoc
34060 Montpellier Cedex, France

R. Madariaga

Sciences Physiques de la Terre, Université Paris VII
75230 Paris Cedex 05, France

Abstract. We study a model of continental collision in which one of the continents acts as a rigid die indenting the other plate which flows as an incompressible viscoplastic medium. We consider two extreme cases of plane deformation: (1) plane strain which corresponds to an infinitely thick lithospheric plate, and (2) plane stress corresponding to a very thin plate. Deformation of the lithosphere, a thick plate, should be intermediate between those extremes. We found that the flow in the plane strain case is quite similar to that obtained by slip line theory. The plane stress results are quite different, since in this case most of the plate shortening is taken up by the thickening of the lithosphere. We also explored the role of boundary conditions on the flow, in particular, the role of the side walls containing the flow of the lithosphere. In the case of a free lateral boundary the main feature is a flow of matter toward this free wall and a S-like pattern for the horizontal stress field. For a rigid wall, on the other hand, the plane strain and the plane stress results are quite different. In the first case, there is a large return flow on the sides of the punch, the material being extruded along the only free surface available. In the plane stress case the return flow disappears, and the material displaced by the penetration of the die tends to thicken the plate. The role of a nonlinear constitutive relation is studied for power law creep. As the power of the flow limit increases, the flow retains its general features, but the deformation localizes creating sharper contrasts between high and low strain rate areas; in plane stress, the effect of nonlinearity is to increase the contrasts in vertical motion. Available data for Asia are discussed in the light of the new results.

Introduction

Plate tectonics, which considers that the lithosphere is divided into a small number of rigid plates interacting only near their common boundaries, can explain many of the global features of the earth. There exist, however, large regions, usually of continental nature, where the lithosphere undergoes large-scale deformation and a rather diffuse seismicity prevails. From its size and tectonic significance, the region of central Asia behind the Himalayan range is one of the most interesting example of intracontinental deformation. Tapponnier and Molnar (1976), observing the chronology and the geometry of the structures in this area, concluded that they had as a common origin the collision between India and Asia at the Himalayas. They went further to recognize that many of the observed features were quite analogous to certain common metallurgical processes, like indentation by a punch and extrusion (Hill, 1950; Backoffen, 1972). They modeled the collision between India and Asia as the plane strain indentation of a rigid-plastic medium by a rigid punch. They justified this interpretation by the analogy between the slip line field associated with indentation and the great strike slip faults observed in satellite pictures of this region. The success of this simple anological model, in spite of its drastic simplification of boundary condition, rheology, etc., encouraged us to make a more detailed study based on continuum mechanics and using modern finite element techniques. A number of authors have used this approach in trying to model lithospheric deformation (i. e., Daignières et al., 1978; Bird, 1978; Bird and Piper, 1980; Vilotte, 1980; Melosh and Raefsky, 1980; P. England and D. McKenzie, personnal communication, 1980). Based on theoretical considerations (Mandel, 1972; Zarka, 1972) and experimental data (Weertman and Weertman, 1975; Ashby and Verrall, 1977), we propose a rigid-viscoplastic rheology for the long-term deformation of the lithosphere. We then study two types of deformation under the action of a rigid punch: plane strain and plane stress. Two alternative numerical methods will be proposed, and their relative merits to solve plane stress or plane strain problems will be analyzed. One is a variational approach; the other is a weighted residuals Galerkin formulation coupled to a penalty function to impose incompressibility. Our results will be discussed in the light of the observations in central Asia that we review in the next section.

Paper number 2B0878.
0147-0227/82/002B-0878$05.00

A review of Indian-Asian collision

We briefly review some observations relevant to the intraplate deformation and geodynamic history of the region of Asia to the north of India. The contact between the Asian and Indian continents was completely established about 30 m.y. ago. Since then, the Indian plate has continued to penetrate into Asia at a mean rate of 3 to 5 cm yr^{-1}. The total shortening of Asia since the beginning of collision is of the order

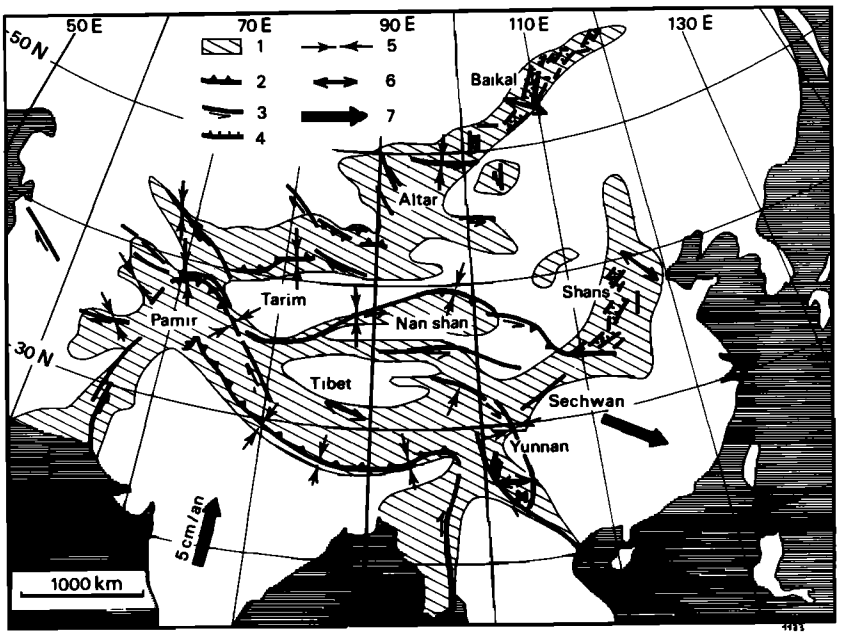

Fig. 1. Simplified map of recent tectonics in Asia (after Tapponnier, 1978): 1, deformation zone; 2, thrust fault; 3, strike slip fault; 4, normal fault; 5, shortening direction; 6, extension direction; 7, plate displacement vector with respect to Asia.

of 1500 km; this leads to an average strain of 30% in the seismically active zone, which has a width of about 3000 km according to Tapponnier (1978). Figure 1, extracted from Tapponnier, shows the main tectonic features of this region:

1. There is a vertical deformation characterized by a crustal thickening which is probably of the order of 40 km (Argand, 1924; Chen and Molnar, 1981; Bird and Toksöz, 1977). This thickening is localized under the Himalayas and in the Tibetan plateau, whose mean altitude is close to 5000 m. The latter presents a number of NS oriented grabens in its southern end where it reaches the highest altitudes (Molnar and Tapponnier, 1978; Ni and York, 1978).

2. The crustal thinning reaches about 10 km under Shansi and Baikal. The latter is probably associated not only with the India-Asian collision.

3. A large horizontal strain exists, which is characterized by the presence of two great strike slip faults systems. To the east are left-lateral strike slip faults whose total slip is very roughly of the order of a few hundred kilometers. To the west is a right-lateral fault system whose accumulated slip is a few tens of kilometers, clearly smaller than the previous one.

These tectonic features are coupled to a regular elevation of the present-day topography: the mean elevation diminishes from the Tibetan plateau toward the Pacific Ocean to the NE.

Considering the geometry of these tectonic structures and the fault plane solutions of shallow earthquakes, we can roughly sketch the stress field in central Asia. In this way we can follow the orientation of the major principal stress axis, which starts with a NS direction to the W of Himalayas, turns progressively to the NW (Mattauer and Mercier, 1980), and finally becomes NW-SE at Tien-Shan and EW at Tadjikistan. To the E and NE of the Himalayas, on the other hand, we observe a different rotation of the principal stress direction: it starts NS on Tibet, then it is NE in Szechwan, and finally returns to NS in Yunnan.

Approximate rheology of the lithosphere

The studies we are going to carry out require an approximation of the average behavior over long periods of time of the lithosphere. It is well established that for periods of time shorter than a characteristic time t_c, the lithosphere behaves eslastically, while for longer times it creeps nonlinearly. This characteristic time is given approximately by $t_c = \mu/K$, where μ is the effective viscosity at a given stress level and K is the elastic rigidity. For different estimates of μ, averaged over a vertical section of the lithosphere, t_c may vary between 10^9 and 10^{12} s, i.e., 10^2 and 10^5 years (Cathles, 1975). Thus for the phenomena associated with continental collision, which extend over several tens of million years, the lithosphere should behave like a nonlinear viscous medium.

The establishment of a constitutive relation requires the definition of stress and strain rate at every point of the continuum. What we need for our purposes however are the values of stress and strain rate ($\underline{\underline{\sigma}}$ and $\dot{\underline{\underline{\varepsilon}}}$, respectively) averaged over certain characteristic volume of medium (Mandel, 1972), i.e.,

$$\underline{\underline{\sigma}} = 1/V \int_V \underline{\underline{\sigma}}^L(\underline{x})\, dV \qquad (1)$$

$$\dot{\underline{\underline{\varepsilon}}} = 1/V \int_V \dot{\underline{\underline{\varepsilon}}}^L(\underline{x})\, dV \qquad (2)$$

where $\underline{\underline{\sigma}}^L$ and $\dot{\underline{\underline{\varepsilon}}}^L$ are local values. The averaging volume is a function of the problem at hand. The 'averaged' strains allow for discontinuous displacements at the local scale, for instance, dislocations, cracks, or faults whose contribu-

tion to the 'averaged' deformation will be integrated inside the reference volume V. The local stress field may be slightly heterogeneous and compatible with local stress concentrations, slip discontinuities, etc., but at the scale of a million years it is averaged over the reference volume. A necessary requirement to replace local stresses by averaged ones is the following energy theorem (Mandel, 1972):

$$\underline{\underline{\sigma}} : \dot{\underline{\underline{\varepsilon}}} = 1/V \int_V \underline{\underline{\sigma}}^L : \dot{\underline{\underline{\varepsilon}}}^L \, dV \qquad (3)$$

With these considerations at hand, we shall refer in the following only to averaged stresses or strains.

Laboratory experiments on lithospheric materials, extrapolated to the pressure and temperature conditions in the earth, have permitted estimation of the strength envelope of the lithosphere as a function of depth (Brace and Kohlstedt, 1980; Kirby, 1980). Using Byerlee's (1978) friction law as the lower limit for fracture and incorporating recent data for the brittle and semibrittle behavior of mantle rocks, Kirby built an approximate strength profile for the lithosphere (Kirby, 1980, Figures 11 and 12, p. 6361). These profiles were calculated for a strain rate of 10^{-14} s^{-1}, which is of the order of what is expected for the geological processes that we are considering here. It comes out of this study that the lithosphere presents a layer of strength to slow deformation that extends between 20 and 70 km for dry olivine or between 20 and 55 km for wet olivine. He also found that the variations in strain rate had little effect on the position of this layer of strength (Kirby, 1980). We accept here that the long-term deformation of the lithosphere is controlled by this layer, which is located mainly in the upper mantle, and that the constitutive relationship of the whole lithosphere for extended period of time will be that of its strongest layer.

The main constituent of the upper mantle being olivine (Goetze, 1978; Ashby and Verrall, 1977), it is usually accepted that its rheology may be approximated by that of olivine. Experimental studies on the deformation mechanisms of single crystals of olivine (Goetze, 1978) and on polycrystalline aggregates like dunite (Post, 1977) or lherzolite (Carter and Ave'Lallemant, 1970) show that the dominant mechanism is nonlinear creep. Therefore, we shall assume in the following that the mechanical behavior of the lithosphere over periods of time extending beyond 1 m. y. is nonlinear creep beyond a certain flow limit, i.e., it is what is usually denominated a rigid nonlinear visco-plastic medium.

In establishing the rigid-viscoplastic law for the lithosphere in this particular case we may define, following Mandel (1972), a mean plastic strain rate $\dot{\underline{\underline{\varepsilon}}}^p$ in the same way as the total strain rate was defined in (2), i.e., as an average over a small reference volume. In this way we do not exclude local elastic strains, provided that they are sufficiently small compared to the overall plastic behavior. In a rigid viscoplastic material as long as the stresses are inside a certain limit surface in stress space, i.e. $F(\underline{\underline{\sigma}}) < 0$, the material remains in equilibrium. Once the stresses are on, or beyond this limit ($F(\underline{\underline{\sigma}}) \geq 0$), plastic flow or creep develops. $F(\underline{\underline{\sigma}})$ is called the flow limit. The strains associated with plastic flow are much more important than elastic strains, which are therefore ignored. For this reason, before the flow limit is reached, the lithosphere is essentially rigid and it may resist stresses reaching up to a few kilobars (McNutt, 1980; Jeffreys, 1976). Beyond the flow limit there may still remain local zones which have not yet reached the plastic limit. Conversely, in regions where the plastic flow limit has not yet been established in the mean, small local pockets may have reached the plastic limit and have undergone contained plastic strains. Thus, the flow limit is a different concept from that of plastic limit. Here we shall assume that it is independent of initial stresses and the history of deformation. Also, under these assumptions the plastic strain rates are compatible, and during flow the volume does not change (trace $\dot{\underline{\underline{\varepsilon}}} = 0$), so that the flow limit is independent of the isotropic stress.

We shall further adpot an associated flow law (i.e., every stress increase during the flow is normal to the flow surface in stress space). From Perzyna (1966) or Zienkiewicz and Godbole (1975),

$$\dot{\varepsilon}^p_{ij} = \gamma < \phi(F) > \partial F/\partial \sigma_{ij} \qquad (4)$$

where γ is the fluidity, ϕ is a function that we shall define next, and the symbol $<\phi>$ means that $<\phi> = \phi(F)$ for $F \geq 0$ and $<\phi> = 0$ for $F < 0$. The flow surface $F(\underline{\underline{\sigma}}, T, \dot{\underline{\underline{\varepsilon}}}^p)$ is a function of stress-strain rate and temperature T. We shall assume here that F depends only on the second stress invariant, J_2; in which case we obtain the well-known Von Mises criterion:

$$F = \sqrt{3}\sqrt{J_2} - \sigma_y \qquad (5)$$

where

$$\sqrt{2J_2} = (S_{ij}S_{ij})^{1/2} \qquad (6)$$

and $\underline{\underline{S}}$ is the deviatoric part of $\underline{\underline{\sigma}}$. Finally $\sigma_y = \sigma_y(T, \dot{\underline{\underline{\varepsilon}}})$ is the flow limit. We may then rewrite (4) in the form

$$\dot{\varepsilon}^p_{ij} = \gamma <\phi(F)> (\sqrt{3}/2\sqrt{J_2}) S_{ij} \qquad (7)$$

As we have already discussed, in this work we shall adopt the power creep law that has been proposed for the flow of olivine under lithospheric conditions, i.e.,

$$\phi(F) = F^n \qquad (8)$$

where n is an integer that may vary between 3 and 5. In the particular case n = 1, we recover a linear viscous flow law. Following Zienkiewicz et al. (1978), we define an equivalent viscosity μ for the lithosphere:

$$\mu = \frac{\sigma_y + (I_2/\gamma\sqrt{3})^{1/n}}{\sqrt{3}\, I_2} \qquad (9)$$

where I_2 is the second invariant of the strain rate tensor:

$$I_2 = \sqrt{2}(\dot{\varepsilon}_{ij}\, \dot{\varepsilon}_{ij})^{1/2} \qquad (10)$$

The plastic flow laws (7) or (9) permit us to represent in a single expression both the rigid-

perfectly plastic flow ($\gamma \to \infty$), in which case,

$$\mu = \sigma_y/\sqrt{3}\ I_2 \qquad (11)$$

and the common power creep law without plastic limit (usually refered to as the Norton-Hoff law), for $\sigma_y = 0$

$$\mu = (I_2/\sqrt{3}\gamma)^{1/n}/\sqrt{3}\ I_2 \qquad (12)$$

In the latter case, (7) may be rewritten also in the form

$$\dot{\varepsilon}^p_{ij} = ((\gamma\ 3^{n-1/2})/2)(\sqrt{J_2})^{n-1} S_{ij} \qquad (13)$$

which is the multidimensional extension of the power law $\dot{\varepsilon} = A\sigma^n$ (Weertman and Weertman, 1975).

The experimental data for high-temperature creep of lithospheric material (Goetze, 1978) show that the local fluidity depends on the temperature T in the form

$$\gamma^L = \gamma^L_0\ e^{-Q/RT} \qquad (14)$$

where Q is an activation energy and R is the universal gaz constant. In order to estimate γ in (4) we integrate over the reference volume V, which in this case will be taken as a layer of thickness L in the lithosphere,

$$\gamma = \frac{1}{L}\int_L \gamma^L_0\ e^{-Q/RT}\ dz \qquad (15)$$

For a given geotherm of the type $T = T_0 + \beta z$ we get

$$\gamma = \frac{\gamma_0}{T_L - T_0}\left[T\ e^{-Q/RT} + \frac{Q}{R}\ E_1\ (Q/RT)\right]^{T_L}_{T_0} \qquad (16)$$

where E_1 is an exponential integral function.

In the numerical models we are going to present we adopted a nonlinear creep law obtained from available experimental data for n and γ of lherzolite, olivine, and dunite, as shown in Table 1. As a reference, we shall also calculate solutions for a linear creep law, in this case we used the value of γ estimated by Weertman (1978) for the Herring-Nabarro creep of olivine. The values of the flow limit σ_y are unknown; lacking experimental data, we adopted three extreme values for the numerical simulations: a very weak σ_y = 600 bars, strong σ_y = 3 kbar, and a very high, physically unreasonable value σ_y = 60 kbar. The latter was used in order to approximate the perfectly plastic case.

Modeling of continental collision

Following the proposition of Tapponnier and Molnar (1976), we shall model continental collision as the indentation of a lithospheric plate by a rigid punch. The lithosphere will be modeled as a rigid viscoplastic medium resting without friction over the asthenosphere. We neglect the interaction between the lithosphere and asthenosphere because the shear stresses associated are probably much lower than those created by collision. The curvature of the lithospheric plate is not considered here nor is the coupling of vertical and horizontal motions. This allows us to treat collision as a two-dimensional plane strain or plane stress problem. Both of these approximations will be considered here.

In order to solve the problem for a finite section of the continental plate we have to impose boundary conditions on the plate limits. These conditions replace the interaction between the studied plate and the neighbouring ones. We shall consider that, to a first approximation, the plate boundaries associated with subduction are approximately stress free. The effect of the punch is replaced by the application of a constant velocity U_o perpendicular to the indented boundary. We limit the region under study by means of artificial boundaries placed sufficiently far from the punch so that the strain velocities are approximately zero. Several of the problems studied here are symmetric about the axis of the punch. This allows us to reduce the size of the finite element grid if we take into account appropriate symmetry conditions about the axis of the indenter.

In order to retain only the main features of the solution and to keep the calculation costs at a minimum, we choose an extremely simplified geometry. We study the flow of a rectangular plate A B C D of 8000 by 5000 km (Figure 2) indented at the center of AB by a punch of width MN (= 2400 km) with a fixed normal velocity U_o. The bounda-

TABLE 1. Estimation of the Fluidity Parameter for two temperature ranges

Rock or Mineral	n	Q,* kJ mol^{-1}	γ_0,** s^{-1} Pa^{-n}	γ, s^{-1} Pa^{-n} 0°-800°C	0°-1200°C
Dunite					
Wet	3.18 ± 0.18	390.00 ± 10.47	1.234×10^{-17}	3.281×10^{-36}	5.719×10^{-29}
Wet	2.4 ± 0.2	334.78 ± 31.42	3.91×10^{-13}	5.122×10^{-29}	6.41×10^{-25}
Dry	4.8 ± 0.4	498.61 ± 69.55	4.777×10^{-29}	4.534×10^{-53}	7.495×10^{-45}
Lherzolite					
Wet	2.3 ± 0.3	334.36 ± 39.38	1.273×10^{-11}	1.669×10^{-27}	2.09×10^{-23}
Olivine					
Dry	3	525.84 ± 21	4.22×10^{-11}	2.74×10^{-37}	1.136×10^{-30}

Estimation of γ from experimental values of power law creep equation parameters (after Weertman and Weertman, 1975). Dunite, Mr Burnett dunite of average grain size of 1 mm, composition is 98; lherzolite, from Australia of average grain size of 0.5 mm; olivine, single crystals from San Carlos (Arizona) peridotite.

* 1 kcal mol^{-1} = 4.19 kJ mol^{-1}.

** 1 kbar = 10^9 dyne cm^{-2} = 100 MN^{-2}.

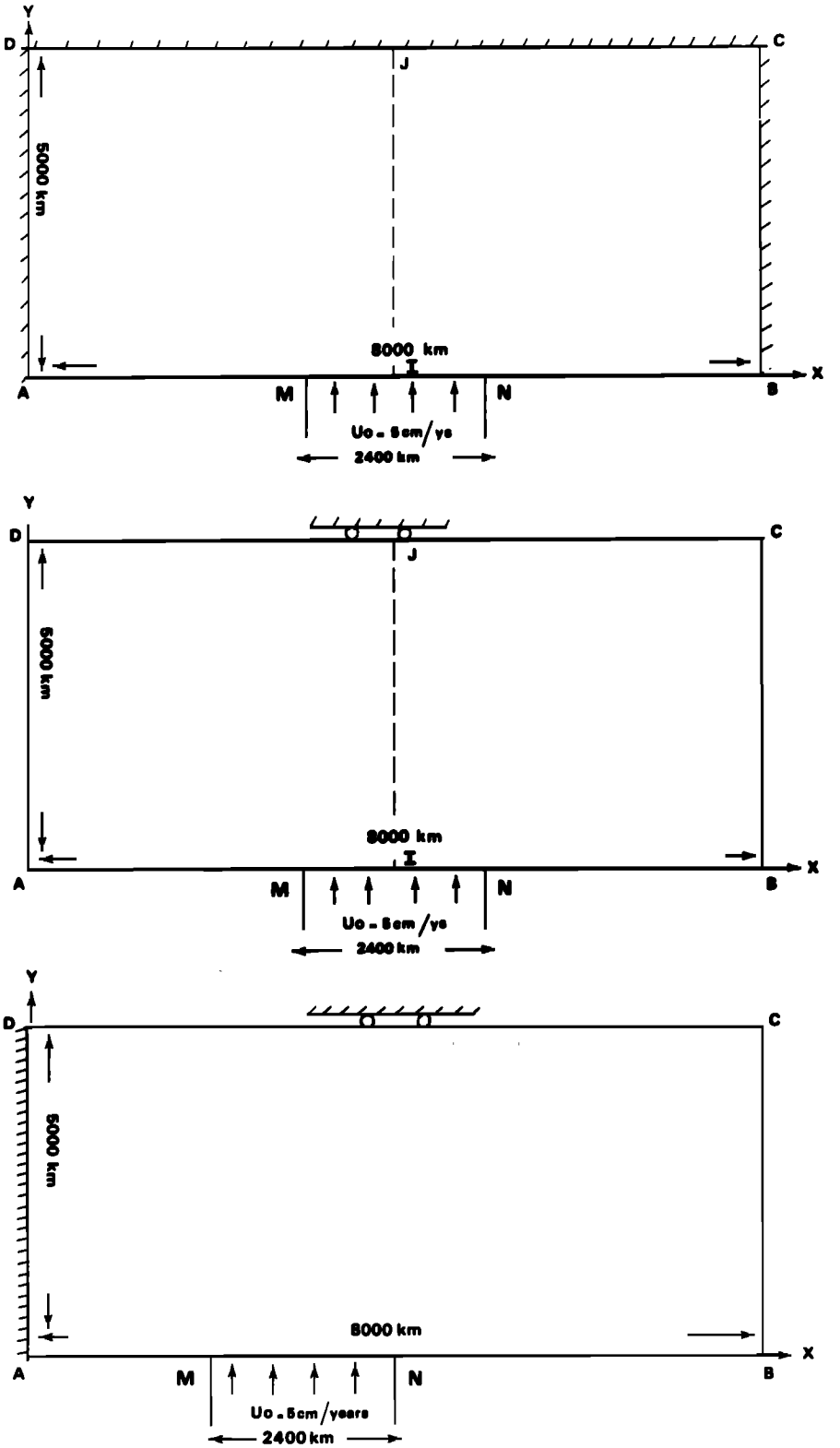

Fig. 2. Geometry of the numerical models. At the top of the fixed side-wall model in which zero velocity boundary conditions are used on AD, DC, and BC. At the center the free lateral wall model. The sides AD, BC are free of stress, and the DC side is free to glide laterally ($\sigma_{xy} = 0$, $v_y = 0$). On AM and NB, stress-free boundary conditions are used, while the indenter MN is simulated by a fixed velocity. In all the calculations, $U_0 = 5$ cm yr^{-1} and MN = 2400 km.

ries AM and NB are stress free. We shall study two possible boundary conditions: (1) velocity is zero for AD, DC, BC; (2) BC and AD are stress free and DC is free to glide laterally. Because of the symmetry about the axis IJ, we study only the IBCJ rectangle in the following.

The rheology was discussed in the previous section. The problem posed in this fashion is an extremely idealized version of the real situation during continental collision. Our main interest is to explore the effect of various parameters and boundary conditions on the flow pattern in the rectangular plate and to discuss the observations in terms of this simple model. The two possible modes of deformation in plane continuum mechanics will be discussed: plane strain and plane stress.

Plane Strain Model

In this case the flow is entirely contained in the x,y plane without a component perpendicular to it. Then

$$\dot{\varepsilon}_{zz} = \dot{\varepsilon}_{yz} = \dot{\varepsilon}_{zx} = 0 \tag{17}$$

and

$$\sigma_{zz} = \frac{1}{2}(\sigma_{xx} + \sigma_{yy}) \tag{18}$$

The stress deviator $\underline{S}$ has two horizontal principal stresses, and the intermediate principal stress is σ_{zz}, which is exactly equal to the isotropic part of $\underline{\sigma}$.

This is the approximation used in the formulation of the slip line method which was used by Tapponnier and Molnar [1976] to analyze continental collision. Their principal argument was the small size of vertical motions when compared to horizontal ones. The main limitation of this approximation is that it does not allow for the presence of regions of elevation, and the only mode of faulting associated with it is strike slip.

Plane Stress Model

In this case the stresses on a plane parallel to x,y are identically zero, and in order to insure incompressibility we have to allow for a vertical strain:

$$\dot{\varepsilon}_{zz} = -(\dot{\varepsilon}_{xx} + \dot{\varepsilon}_{yy}) \tag{19}$$

In this model there exists the possibility of vertical velocities and plate thickening. It does also have the advantage that the effect of gravity may be incorporated in it, although it will not be considered here but will be left as a subject of future research.

The solution of the problem we have posed may only be obtained with numerical methods. We have chosen a finite element technique because of its flexibility in dealing with nonlinear constitutive laws. We have used two different formulations of the finite element method in order to solve the two modes of plane deformation that we have studied. In the first, a weak formulation of Galerkin's method was used to solve plane strain problems. A penalty function was introduced to approximate incompressibility. In this way we can study without difficulty both stress and velocity boundary conditions. This method has clear advantages over stream function formulations, which present problems in dealing with stress-free boundaries. The second formulation was used to study plane stress problems. This method, proposed by Daignières et al. [1978], uses a variational principle for the power dissipated by the flow and is based on the theory of convec functionals.

Results

We have solved the indentation of the rectangular plate for two types of rheology: a rigid-viscoplastic medium and a Norton-Hoff (power law creep) medium. For the rigid-viscoplastic medium we explore the role of the different parameters σ_y, n, and γ appearing in the constitutive relation (9). For the Norton-Hoff law (12) we vary both n and γ. While the results are entirely comparable, from a numerical point of view we found that the Galerkin approach described in Appendix A is more efficient for plane strain problems. The method of Appendix B was more economical in dealing with plane stress problems. In the following we discuss separately the results obtained for each of the two modes of deformation. In every case, we studied the role of the boundary condition on the border BC of the rectangular plate (see Figure 2), the influence of the nonlinearity of the creep law (for n = 1, 3, and 5), and the influence of the flow limit σ_y (0.6, 3, 60 kbar).

The numerical solutions were all calculated for an indenter velocity U_o = 5 cm yr^{-1} and width L = 2400 km. The solutions may be scaled to other values of U_o and L, noting that they are controlled by two nondimensional numbers: the index n of the nonlinear creep law and the ratio:

$$K = \frac{\sigma_y}{(U_o/\gamma L)^{1/n}} \tag{20}$$

that represents the ratio between the yield strength and a representative value of the creep stress. We may write the solutions in the following nondimensional forms:

$$\begin{aligned} x &= Lx' \\ u &= U_o u'(K,n) \\ \dot{\varepsilon} &= (U_o/L)\,\dot{\varepsilon}'(K,n) \\ \sigma &= (U_o/\gamma L)^{1/n}\,\sigma'(K,n) \end{aligned} \tag{21}$$

The nondimensional primed functions depend only on the nondimensional numbers n and K. If $\sigma_y = 0$, K = 0 and the numerical solutions depend only on n. Velocities and strain rates depend on γ only through K. Stresses, on the other hand, scale like $\gamma^{-1/n}$ and are very sensitive to this parameter, which in our opinion is still poorly known for the lithosphere. The values of γ used in the calculation were calculated averaging the γ shown in Table 1; we found $\gamma = 10^{-23}$ s^{-1} Pa^{-1} for n = 1, $\gamma = 2.74\ 10^{-37}$ s^{-1} Pa^{-3} for n = 3, and $\gamma = 4.53\ 10^{-53}$ s^{-1} Pa^{-5} for n = 5. The solutions may be easily rescaled to other values of γ using (20) and (21).

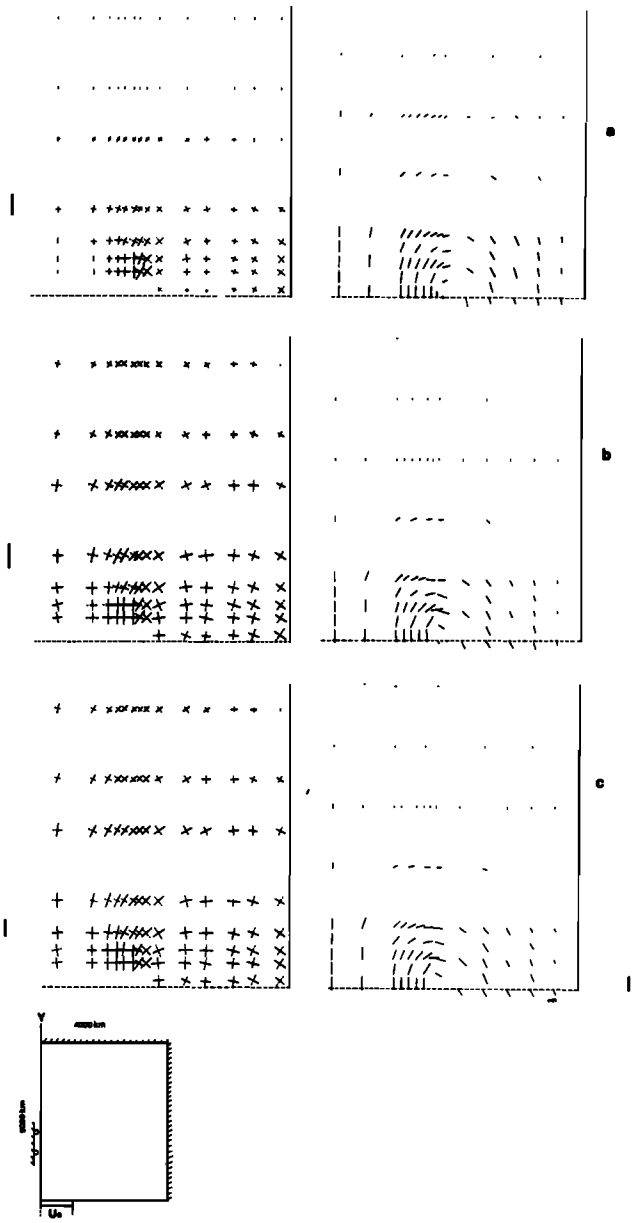

Fig. 3. Plane strain results for fixed boundary conditions on BC, the model at the top of Figure 2. Deviatoric stress field (left) and velocity field (right) are shown for (a) n = 1, $\gamma = 1\times10^{-23}$ s^{-1} Pa^{-1}; (b) n = 3, $\gamma = 2.74\times10^{-37}$ s^{-1} Pa^{-3}; (c) n = 5, $\gamma = 4.53\times10^{-53}$ s^{-1} Pa^{-5} with a yield stress σ_y = 600 Pa (60 bars). The corresponding stress ratios are (a) K = 0.1, (b) K = 0.5, (c) K = 0.35. The stress field (left) is described by the principal stresses, with the solid line indicating the maximum compressional axis (σ_1) and the dotted line, the minimum compressional axis (σ_3). The stress scale is indicated by the short bars to the left of the figures. The bar next to (a) represents 100 bars, the one next to (b) is 1 kbar; bottom one equals 10 kbar. Velocities are shown as vectors on the right, the scale is given by the short bar at the bottom right which measures 5 cm yr^{-1}. Stresses were calculated at the integration points of the numerical grid, while velocities were obtained at the nodal points; this is why they are shown at different places on the grid.

Plane Strain Results

Influence of the boundary condition on the side BC. Figures 3 and 4 show the deviatoric stress and velocity fields for the two possible boundary conditions on BC: rigid boundary (Figure 3) and free boundary (Figure 4). In both we show, from the top, the results obtained for the power laws n = 1, n = 3, and n = 5, the corresponding values of γ are listed in Table 1. A very low value of σ_y = 60 bars was used in these calculations.

The results for these two boundary conditions are quite different. The stress field is shown at

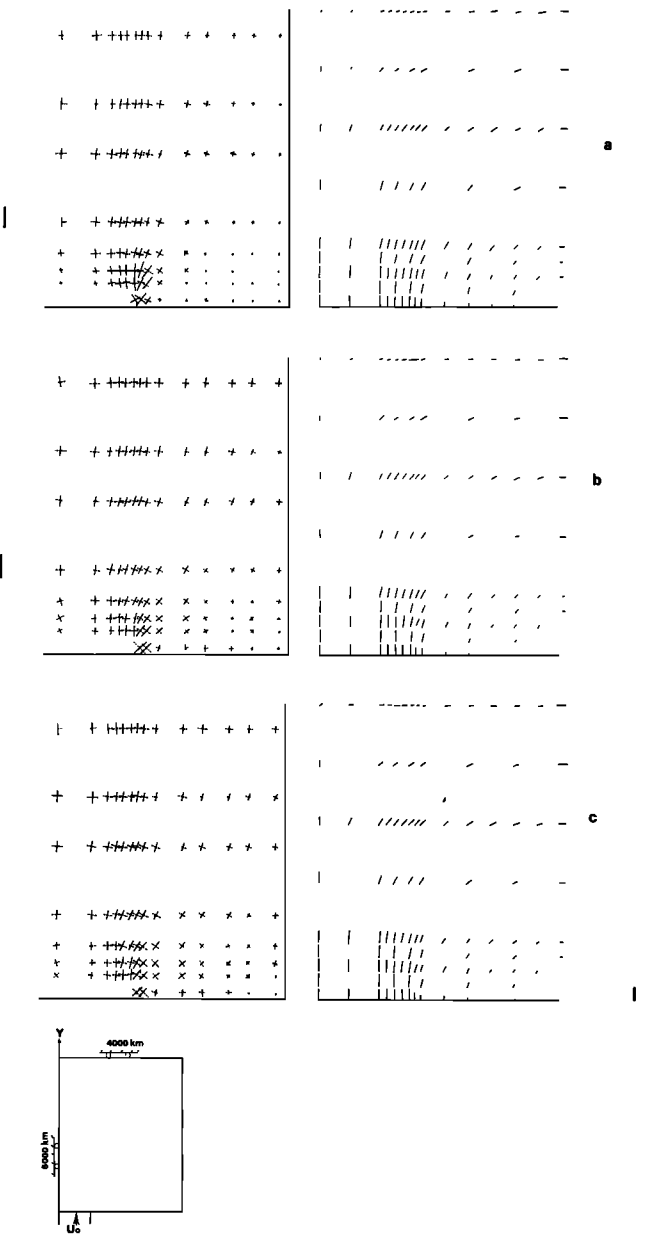

Fig. 4. Plane strain results for free boundary conditions on BC, the middle model in Figure 2. Deviatoric stress field (left) and velocity field (right) are shown in the same way and for the same parameters as in Figure 3.

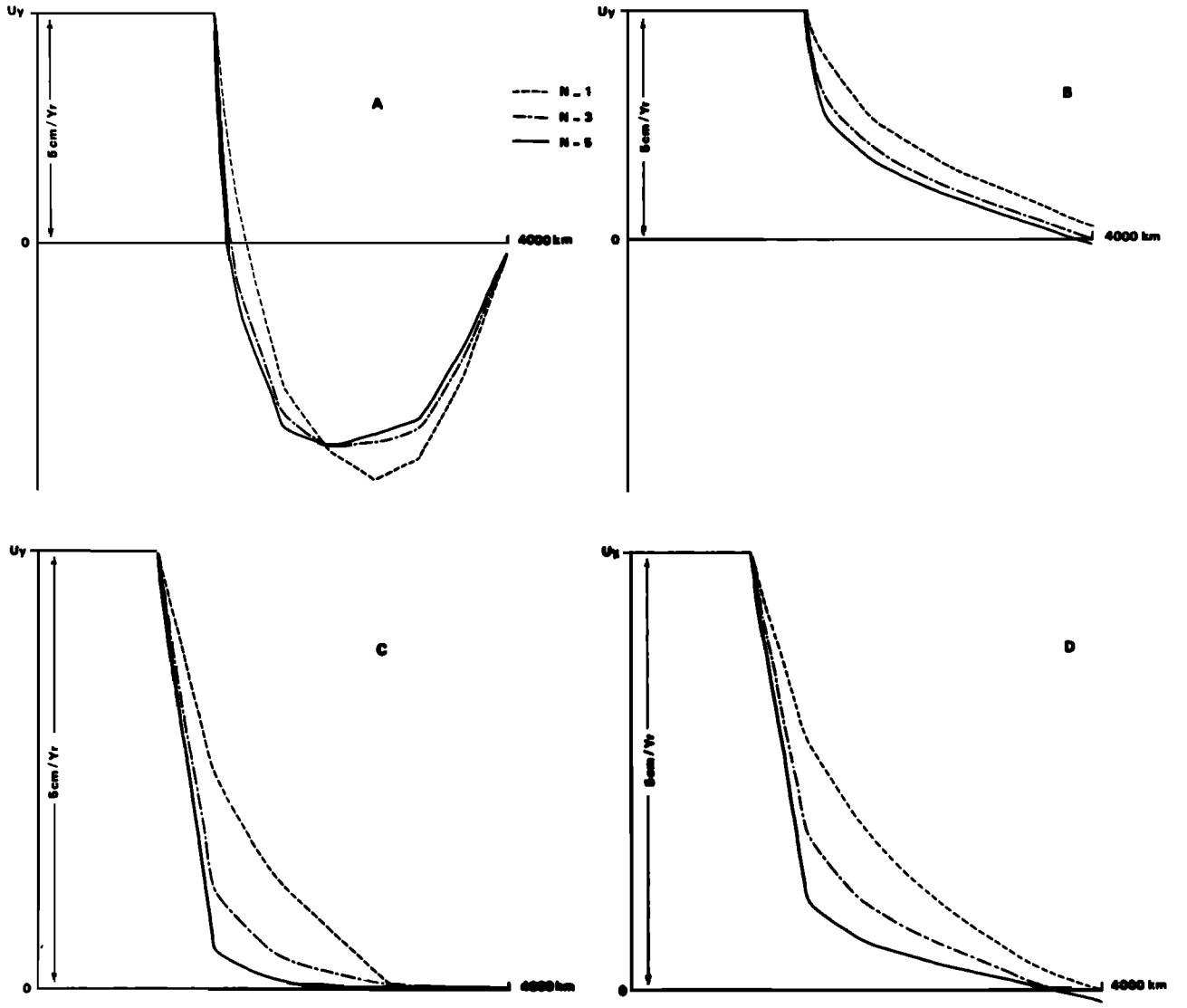

Fig. 5. Free surface velocity on the sides of the punch, calculated for (a) plane strain for fixed boundary conditions on BC, (b) plane strain for free boundary conditions on BC, (c) plane stress for fixed boundary conditions on BC, and (d) plane stress for free boundary conditions on BC. Results are shown for n=1, 3, and 5.

the left of both figures. In plane strain the two horizontal principal deviatoric stresses are equal and of opposite sign, in the figures the solid line is the compressive axis and the dotted line, the extensive one. When the boundary BC is rigid (Figure 3), the stresses rotate by a full 90° as one moves away from the punch into the material and out to the right toward the rigid boundary BC. To the right of the punch, the tensional axis becomes perpendicular to the punch front. The results are thus very similar to those reported by Tapponnier and Molnar (1976) for slip line theory. A very different result is obtained when BC is stress free. In this case, the compressional stress in front of the punch rotates by 20° to the E, then passes through an inflexion point and becomes eventually normal to the back wall describing an S-like pattern. These results are new and interesting since they may be confronted with the stress directions obtained by Mattauer and Mercier (1980) from a number geological observations.

For the velocity field the difference between the two boundary conditions are even more dramatic. For the fixed boundary (Figure 3, right), incompressibility forces the material to 'escape' along the free surface on both sides of the punch. The velocity vector rotates sharply by about 180° in the vicinity of the edge of the punch. Numerical experiments showed that this motion toward the free surface depends strongly on the incompressibility. It disappeared as soon as a weak compressibility was introduced. Ahead of the punch, we observe a region that undergoes an almost rigid translation. This zone has a triangular shape that closely corresponds to the dead triangle found in the slip line solution of this problem. When the boundary BC is free (Figure 4), the velocity vector rotates only by 90° so that the material moves lateraly parallel to the punch

front and escapes lateraly through the BC walls. The rigid block in front of the punch is larger than for a rigid wall BC. Thus it appears as if the material was being squeezed laterally through BC with a minimum of rotation.

Influence of nonlinearity of the constitutive equation. The influence of nonlinearity is similar for both types of boundary conditions on BC. As the nonlinearity increases from n = 1 to n = 5, we observe a progressive concentration of strain rate near the punch in the same regions where stresses concentrate. There are larger zones where there is practically no strain rate, i.e., that move like rigid blocks. The return of material in the case of the rigid wall BC tends to concentrate closer and closer to the punch as n increases, as is clearly seen in the surface velocity plots on Figures 5 and 6.

While the value of the velocity appears to be mainly controlled by the velocity of indentation, the stresses are very sensitive to the degree n of the nonlinear law. For n = 1, stresses are of the order of tens of bars, while for n = 5 they reach several kilobars (Vilotte and Daignières, 1981; Neugebauer et al., 1981). For n fixed, the stress field is, of course, very sensitive to the value of γ, which depends, in turn, on the activation energy Q and the thermal structure of the lithosphere (see equation (16)). For instance, a variation of 200 °K at the base of the lithosphere, for an activation energy of 530 kJ mol^{-1}, creates for n = 3 a variation of a factor of 20 in the stresses.

Influence of the plastic limit. Keeping n = 3 and $\gamma = 2.74 \times 10^{-37}$ s $kbar^{-3}$ as constants, we explore the effect of changing σ_y from 0.6 to 3 to 60 kbar. The last value was adopted only to study the influence of σ_y and has no geophysical applicability in itself. For a fixed boundary BC we find that the geometry of the results are very sensitive to σ_y. We note (Figure 7) that the maximum return flow across the free surface concentrates near the punch as σ_y is increased. We also observe that the transition between the zones undergoing large strains (10^{-14} $s^{-1} > \dot{\varepsilon}^p > 10^{-15}$ s^{-1}) and those that remain practically rigid ($\dot{\varepsilon}^p < 10^{-17}$ s^{-1}) gets sharper with increasing σ_y. Thus, the effect of σ_y is similar to that of increasing n since in both cases the nonlinearity of the law is increasing.

In the case of a free boundary BC, the role of σ_y is also very important and produces the same effects as above: a progressive concentration of strains in the vicinity of the punch as σ_y increases.

Plane Stress Results

In Figures 8 and 9 we present the horizontal deviatoric stresses and the horizontal velocity vectors calculated under the conditions of plane stress by means of the method described in Appendix B.

The horizontal principal deviatoric stresses in this case are not equal and opposite as in plane strain, and the incompressibility is insured by the vertical thickening or thinning of the plate. This allows for a larger variety of features in the plane stress problem.

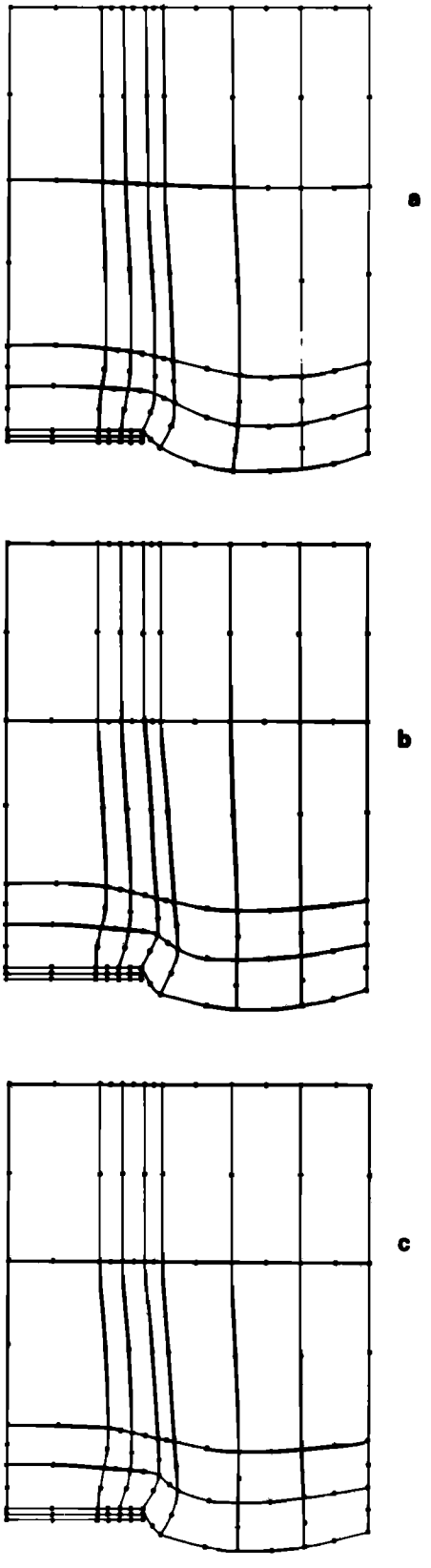

Fig. 6. Deformed grid after 10^6 yr of steady indentation in plane strain with rigid wall boundary condition on BC and an indenter velocity of 5 cm yr^{-1}. (a), (b), and (c) refer to the same parameters as in Figure 3.

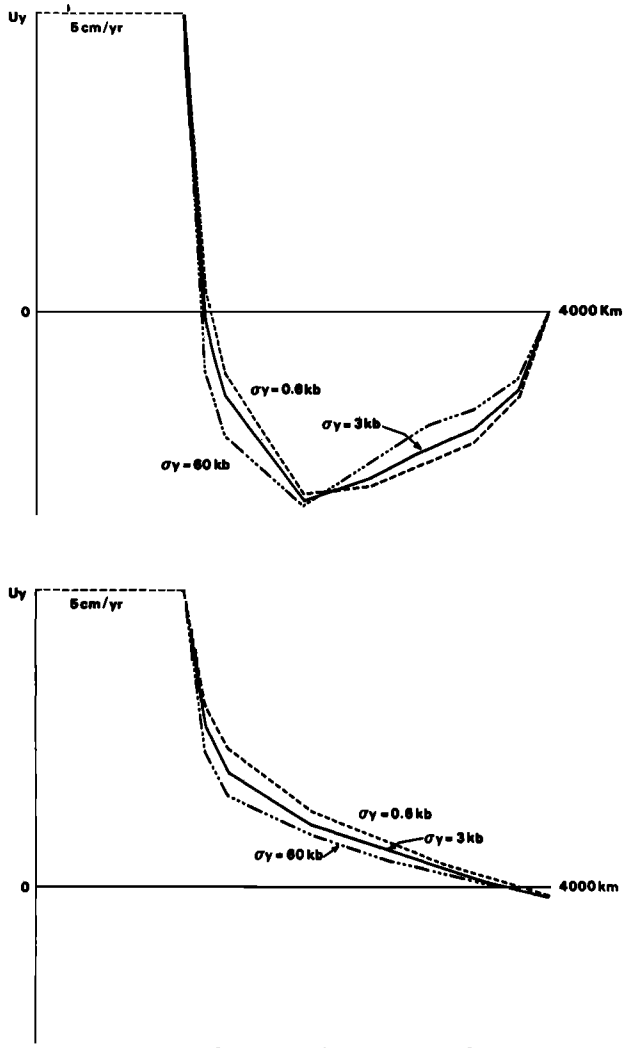

Fig. 7. Effect of σ_y on the free surface velocity for the plane strain case with fixed boundary conditions on BC (top), and free boundary conditions on BC (bottom). A creep law with n = 3, $\gamma = 2.74\times10^{-37}$ s^{-1} Pa^{-3} was used. The yield stresses are σ_y = 0.6 kbar (K = 0.2), σ_y = 3 kbar (K = 1), σ_y = 60 kbar (K = 20).

Influence of boundary conditions on the border B.C. In the rigid BC boundary case (Figure 8) we observe that the compressional stress, which is initially parallel to the direction of advance of the indenter, turns to the right and and rotates clockwise by 45° as one moves laterally and away from the punch. In the case of the free BC wall (Figure 9) the compressive stress makes the same S-like sideways turn that was observed in plane strain. Comparing with the plane strain solution now, the results are quite different in the case of a fixed BC wall (cf. Figures 3 and 8). This is because in the plane stress model, incompressibility is achieved by a vertical strain $\dot{\varepsilon}_{zz}$; there is no horizontal incompressibility and the large return flow at both sides of the punch that was so visible in plane strain disappears. On the other hand, the relative values of the principal stresses change rapidly passing from a large horizontal extension parallel to the punch to a large horizontal compression in the same direction as one moves away from the free surface next to the punch. In the case of the free wall BC the geometry of the horizontal flow is very similar in plane strain and plane stress (cf. Figures 4 and 9), the main effect of the indentation being to push the material laterally across BC.

When we study the horizontal velocities, we reach the same conclusion: there is practically no influence of the mode of deformation when the boundary BC is free. The main feature is a rotation of velocity by 90° away from the punch. If the boundary BC is a rigid wall, on the other hand, the plane stress results (Figure 8) are very different from those in plane strain (Figure 3). While in plane strain, the major feature was the return flow on the sides of the punch; under plane stress we observe velocities which are parallel to the motion of the punch (Figure 5). The material is squeezed vertically thickening the plate (see below and Figure 11).

State of stress. As already mentioned, in plane stress there may be different stress regimes depending on the relative sizes of the principal stresses. In fact one of the principal stresses is zero and vertical, while the two others are on the plane. Depending on whether the vertical stress is the greatest, the intermediate, or the least principal stress, one has different stress regimes. This is the state of stress that prevails in the layer of strength of the lithosphere, but we shall assume that it also controls the type of tectonics that will affect the brittler surface layer. Under this assumption we define reverse, strike slip, and normal faulting zones in Figure 10 for fixed and free boundary BC and two values of the power law n. We clearly see in all the examples that there is a well-defined reverse faulting zone in front of the punch (1 in Figure 10). The extent of this zone depends on the boundary conditions, it is narrower and deeper for the free lateral boundary than for the rigid one. Outside this zone most of the plate is characterized by an intermediate vertical principal stress, the stress condition for strike slip faulting. We also notice to the right of the punch two zones of extension (normal faulting) along the free surface. This region extends also along the side wall BC when this is free of stress.

Vertical motions. We have calculated the vertical strain rates for all the plane stress models. In Figures 11 and 12 we show three-dimensional plots of the vertical strain calculated for both types of boundary conditions on BC. The most important feature of the vertical strain is the broad thickening (positive vertical strain) zone in front of the punch. Strain rates there reach values of the order of $(1\text{-}3)\times10^{-8}$ yr^{-1} which are of the order of the reference strain rate of 2.5×10^{-8} yr^{-1} calculated dividing the velocity by the width of the indenter. The vertical strain rate presents concentrations near the edges of the punch, which appear as peaks in Figures 11 and 12. These are due to the abrupt change in boundary conditions across the punch edge, i.e., fixed velocity inside the punch and free surface outside the punch. Stress concentrations of this type are known to appear in all mixed boundary value problems like this one. In the elastic case the strain presents an inverse

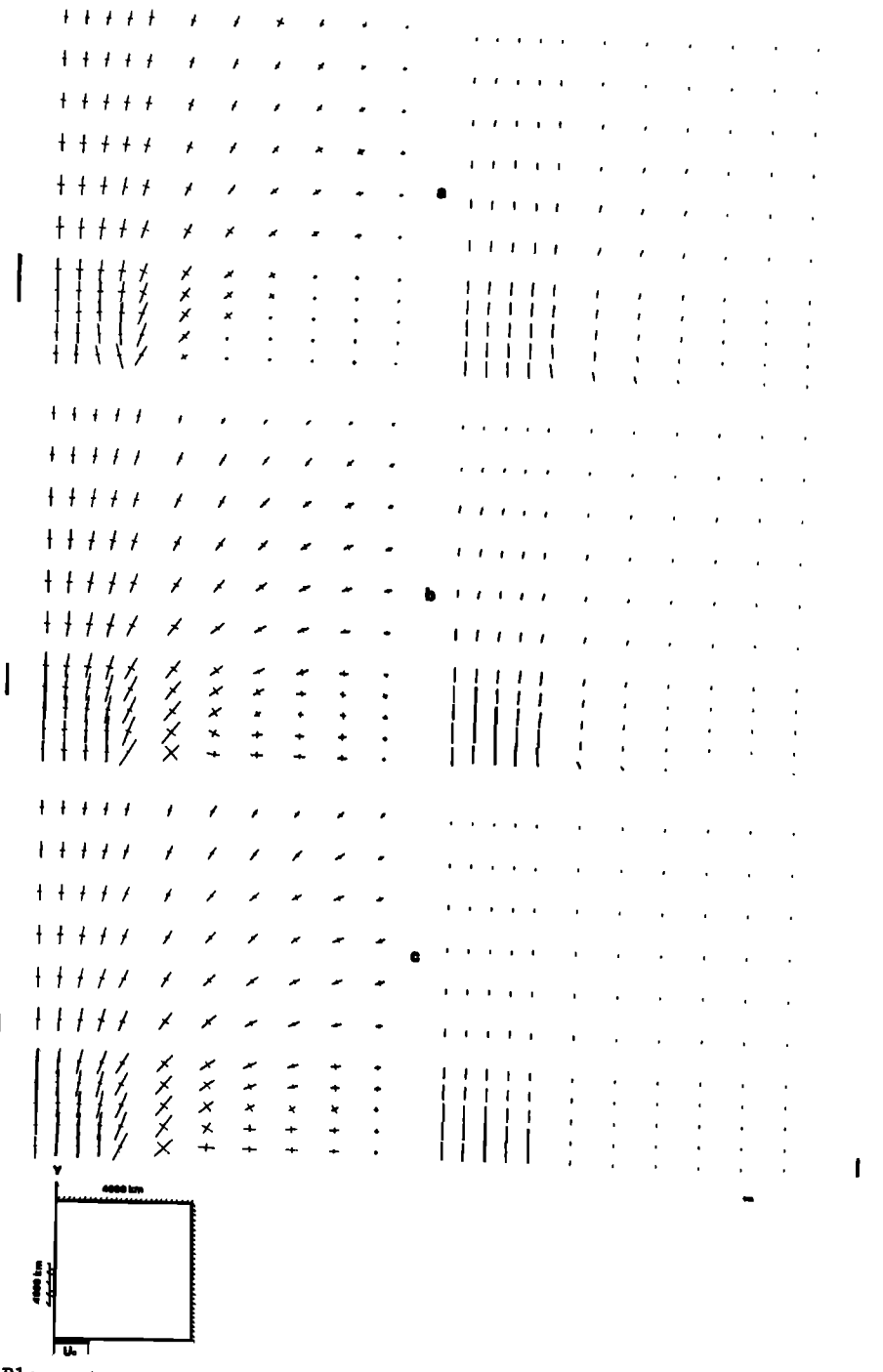

Fig. 8. Plane stress results : horizontal deviatoric stress field (left), and horizontal velocity field (right) for rigid wall boundary condition on BC. Same parameters as in Figure 3. The stress scale is given by the short bars to the left of the figures which represent 100 bars, 100 bars, and 10 kbar from top to bottom. Velocity scale is given by the short bar at the right which measures 5 cm yr^{-1}.

square root singularity inside the punch that is of the same type as the stress concentration associated with crack edges in fracture mechanics. These concentrations are smoothed here by plastic behavior and would be further reduced by a smoothing of the punch geometry. They would, however, be always present, and it would be very interesting to try to identify them in the geological maps of Tibet. To the sides of the punch there are regions which are undergoing thinning with vertical strain rates of up to -2×10^{-10} yr^{-1}.

This is presented in a more quantitative form in the plots of Figure 13, where vertical strain rates zones are identified by different shadings. The vertical strain rates may be converted into vertical velocities if one makes an assumption about the thickness of the plate. As discussed in the section on rheology, the effective thickness

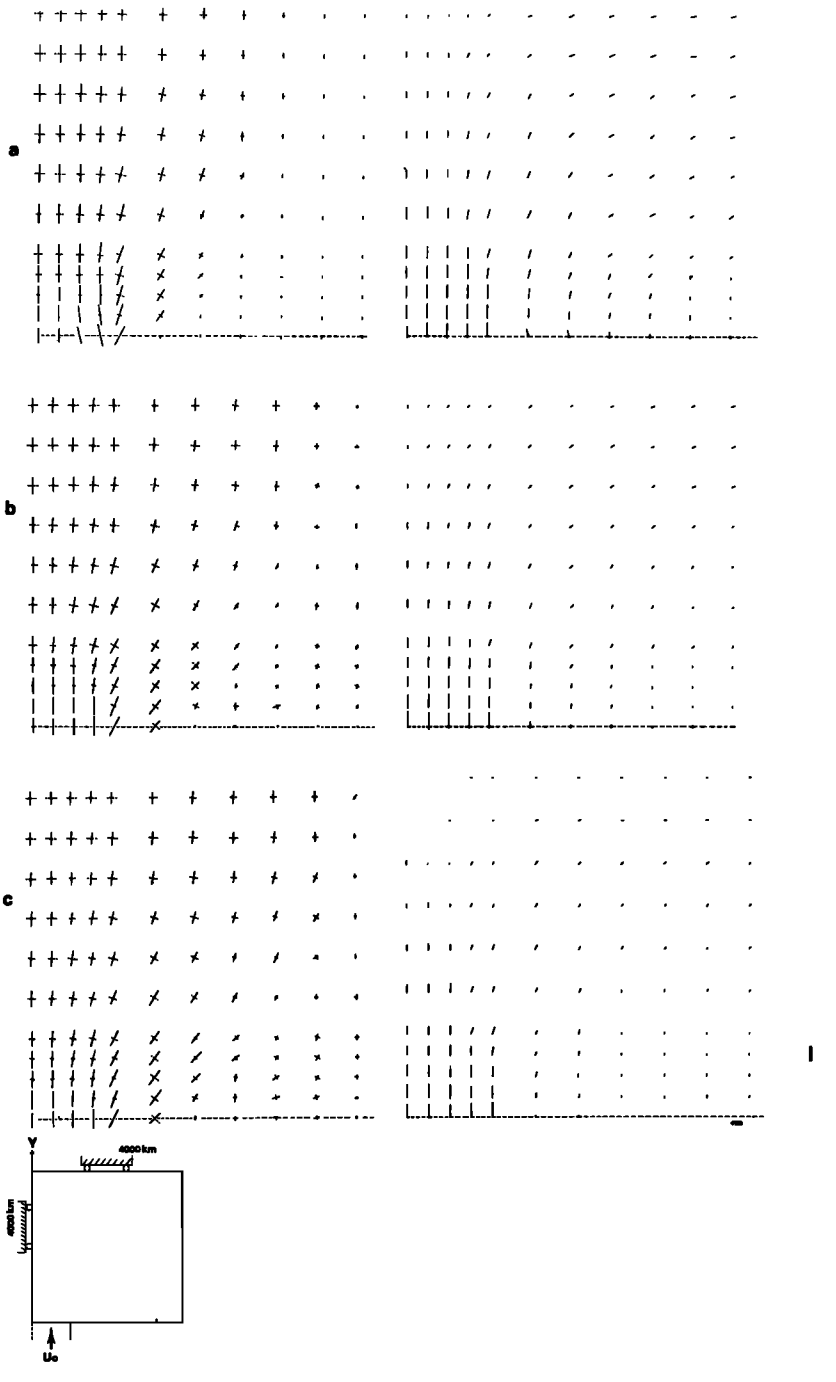

Fig. 9. Plane stress results: horizontal deviatoric stress field (left) and horizontal velocity field (right) for free boundary condition on BC. Same parameters as in Figure 3. The stress scale is given by the short bars to the left of the plots, they represent 100 bars, 200 bars and 10 kbar from top to bottom. The velocity scale is given by the short bar at the right which measures 5 cm yr^{-1}.

of the plate is that of the layer of strength of the lithosphere: 50 km for dry olivine, 35 km for for wet olivine. Calculating surface elevation velocities requires further assumptions about isostatic compensation which may seem premature to introduce here without consideration of gravity.

Let us note, finally, that the thickening region penetrates deeper in the case of the rigid sidewall. In all the examples we have a rather flat thickening zone in front of the indenter which is tempting to relate to the Tibetan plateau in the case of the Himalayan collision. The thickening zone disappears more or less abruptly as a function of the index n of the creep law. The higher n is, the sharper is the boundary between the plateau and the rest of the plate.

Influence of nonlinearity. The influence of nonlinearity may be characterized, as in the case of plane strain, by a sharpening of the bounda-

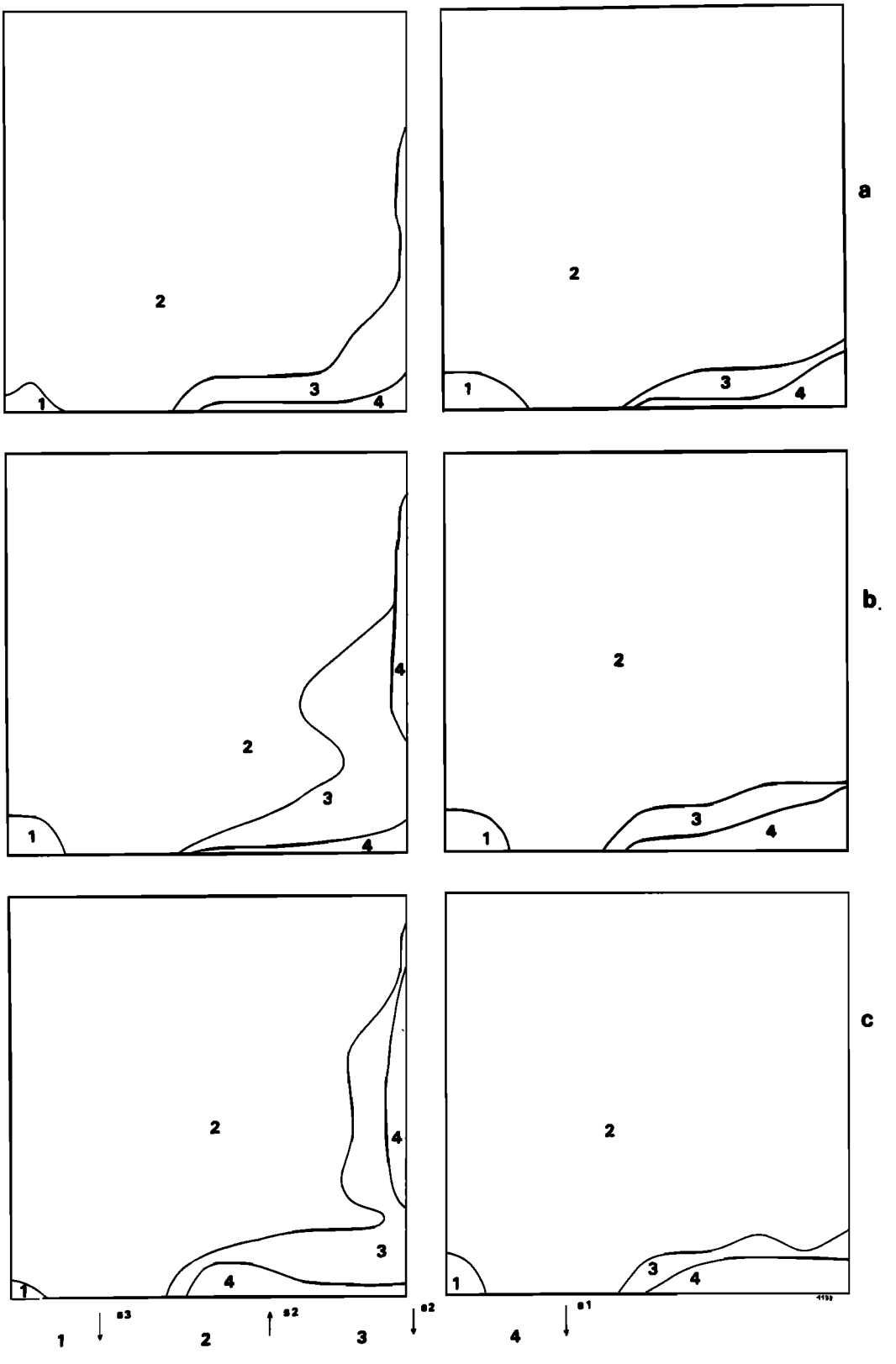

Fig. 10. Deviatoric stress state (type of faulting) for plane stress indentation. (a), (b), and (c) refer to the parameters described in Figure 3. (left side) Free boundary condition on BC. (right side) Rigid wall boundary condition on BC: 1, vertical minimum deviatoric stress, the condition favoring reverse faulting; 2 and 3, vertical intermediate principal stress axis, the condition for strike slip faulting; 4, vertical maximum principal stress, the condition for normal faulting.

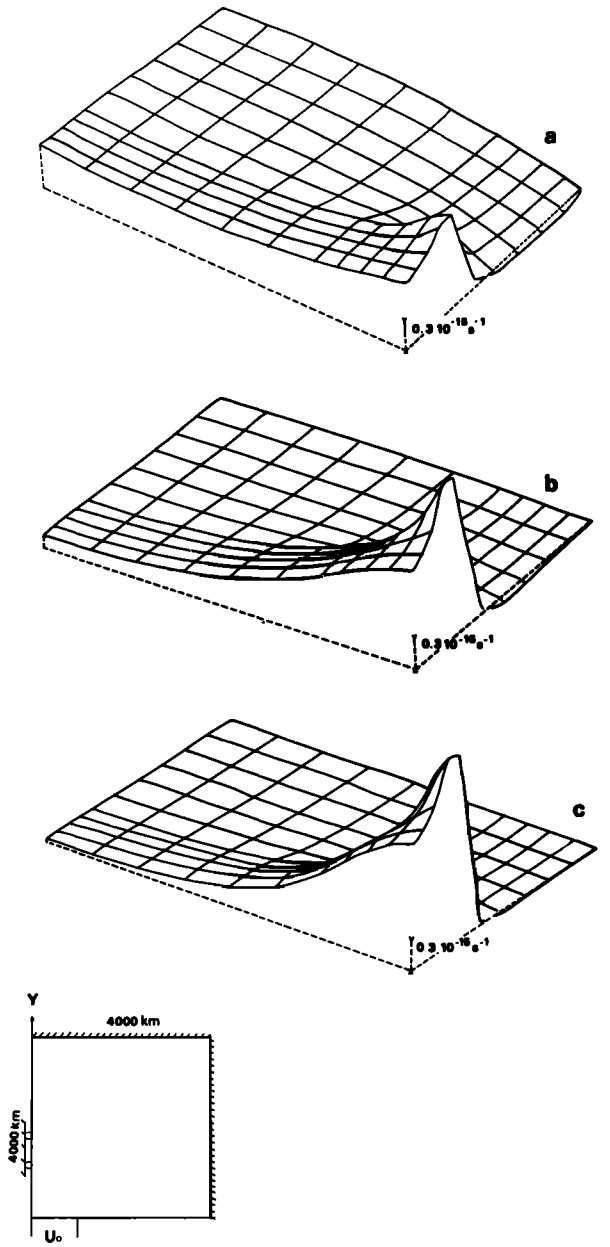

Fig. 11. Three-dimensional plot of vertical strain rate for plane stress for rigid wall boundary condition on BC. (a), (b), and (c) refer to the parameters listed in Figure 3.

ries between strongly deforming and more or less rigidly moving areas of the plate. This is clearly illustrated by the velocities of the free surface on the side of the punch shown in Figure 5. Another interesting effect of n is the slightly negative horizontal component of the velocity near the edge of the punch when n = 1. This component becomes positive (movement away from the punch) for n ≥ 3 when BC is free. For the rigid BC wall the velocity is inward (negative) near the punch edge even for n = 3. As for plane strain, the stresses vary dramatically with n, while the values of the velocities remain essentially controlled by the velocity of penetration of the punch.

For the vertical motion, nonlinearity tends to concentrate it closer to the punch and gives an increased amount of thickening. At the same time the topography decreases faster when one moves away from the punch in the nonlinear case (Figures 11 and 12).

The geometry of the possible tectonic zones depends also on n. The region of possible thrusting which is confined to the front of the punch in the linear case extends significantly for n = 5 (Figure 10). Similarly, the extension (normal faulting) zone increases slightly with n.

An asymmetric example. The examples studied so far were symmetric about the punch axis. We studied an asymmetric example with a rigid side wall to the left and a free wall to the right. The results for the plane stress case are shown in Figure 14. Here the arrows represent the instantaneous velocities at four successive times.

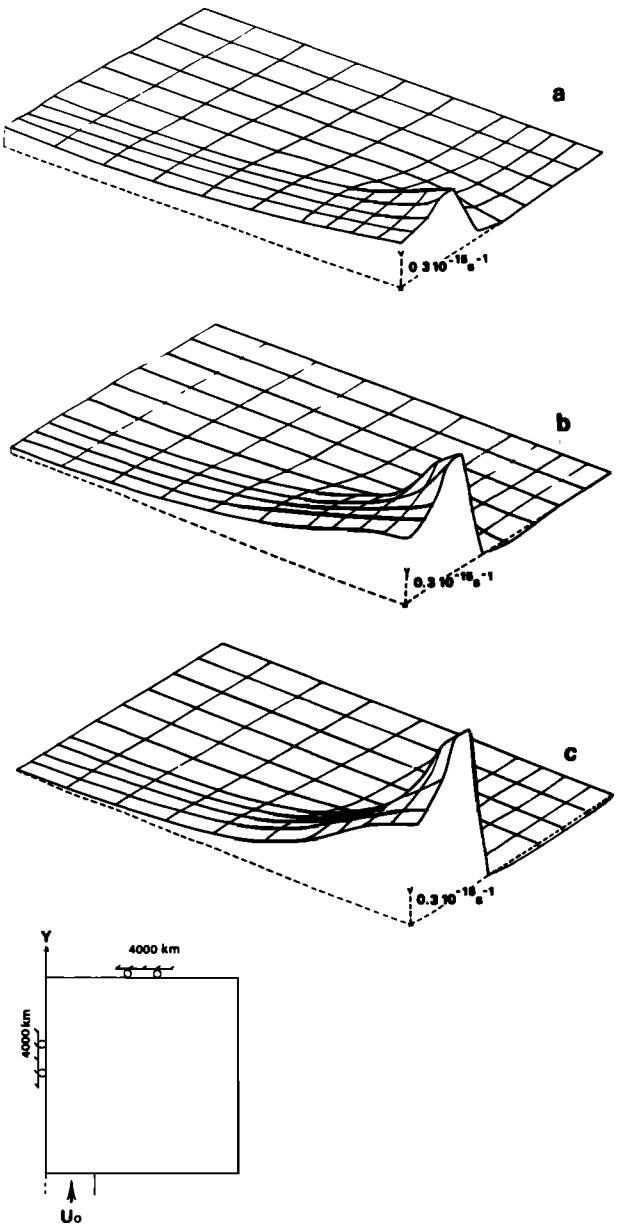

Fig. 12. Three-dimensional plot of vertical strain rate for plane stress for free boundary condition on BC. Same parameters as in Figure 3.

The integrated effect of the velocity field is taken into account by recalculated grid indicated by the dotted lines. The velocity field changes very little with time. Its main feature is the lateral motion of material to the right, through the BC wall. The thickening due to this model is shown at the bottom of Figure 12. It is clear from these two figures that the dominant features of the solution, to the right of the punch, are those of the symmetrical free BC boundary problem; while to the left, the solution is very similar to the fixed side wall solutions.

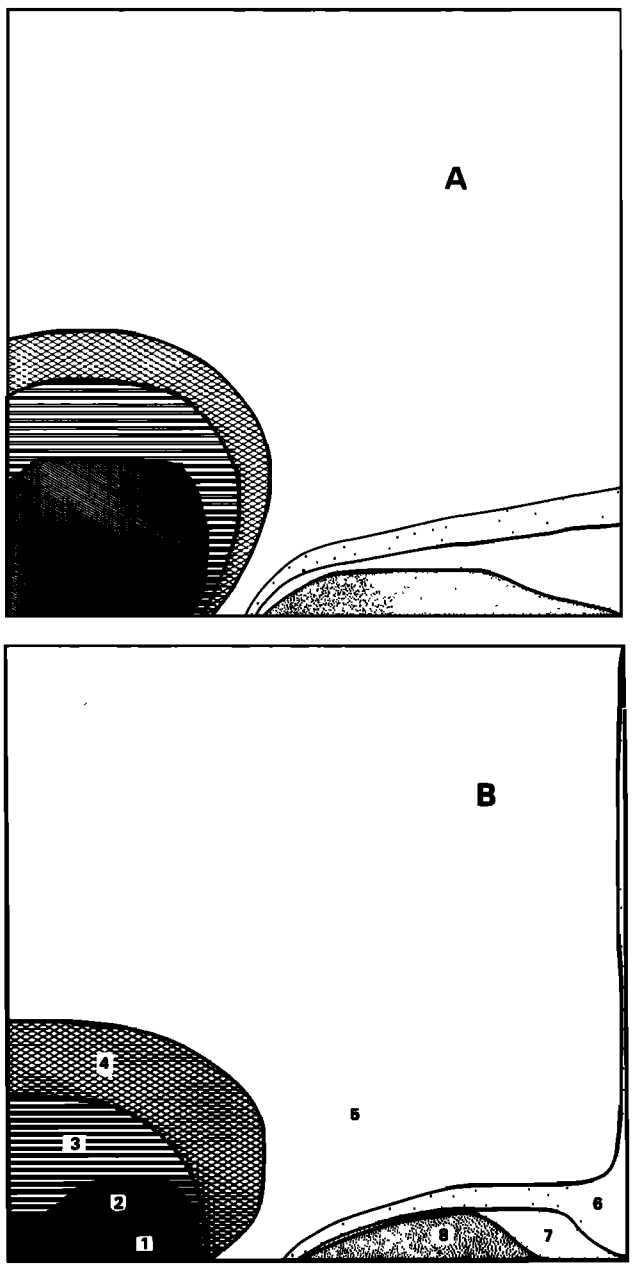

Fig. 13. Vertical strain rate for the plane stress case, with n = 3 and an indenter velocity U_0 = 5 cm yr^{-1}. These solutions are independant of γ. (a) Rigid wall boundary condition on BC; (b) Free boundary condition on BC; (c) Asymmetric case. The shading indicates the vertical strain rate $\dot{\varepsilon}_z$: 1, $\dot{\varepsilon}_z > 2 \times 10^{-8}$ yr^{-1}; 2, $2 \times 10^{-8} > \dot{\varepsilon}_z > 1 \times 10^{-8}$ yr^{-1}; 3, $1 \times 10^{-8} > \dot{\varepsilon}_z > 0.3 \times 10^{-8}$ yr^{-1}; 4, $0.3 \times 10^{-8} > \dot{\varepsilon}_z > 0.1 \times 10^{-8}$ yr^{-1}; 5, $0.1 \times 10^{-8} > \dot{\varepsilon}_z > 0$ yr^{-1}; 6, $0 > \dot{\varepsilon}_z > -0.9 \times 10^{-10}$ yr^{-1}; 7, $-0.9 \times 10^{-10} > \dot{\varepsilon}_z > -2 \times 10^{-10}$ yr^{-1}; 8, $-2 \times 10^{-10} > \dot{\varepsilon}_z$.

Discussion

We have presented numerical results for the two-dimensional flow of a rigid nonlinear viscoplastic material, driven by the penetration, at a fixed velocity, of a rigid indenter. This model was proposed by Molnar and Tapponnier (1975) to explain the deformation of Asia due to the collision with India. Tapponnier and Molnar (1976) studied this model with slip line theory, which applies only to plane strain (no vertical motion) deformation of a rigid-plastic material. In this paper, we studied the deformation of a continental lithospheric plate under both plane strain and plane stress conditions and for more realistic power law creep of the lithosphere. Under plane strain there is no vertical velocity, and therefore one may not study the thickening of the lithosphere, which is one of the possible origins of Tibet. Also in this case, the vertical stress is equal to the isotropic stress and is the intermediate principal stress. The least and greatest principal stresses are horizontal, and the only mode of rupture that we would normally associate with plane strain is strike slip.

The other mode of deformation we studied is plane stress in which the vertical stress is exactly zero. This is the mode of deformation of a very thin plate. There are no simplified methods, like slip line theory, to solve plane stress plasticity problems; only numerical solutions are possible. Under plane stress, incompressibility is assured by vertical strain, i.e., thickening or thinning of the lithosphere. Also, the greatest and least principal stresses are not confined to the plane of the plate, so that states of stress compatible with normal and thrust faulting are possible. Our results are strictly valid for the layer of strength of the lithosphere that according to Kirby (1980) lies between 20 and 50 km (or 70 km) depth. At shallower depths the crust is brittle and fractures under the driving action of the stresses in the deeper layer of strength.

The lithosphere is, of course, a thick plate which does not deform in either pure plane strain or plane stress. From the results of plate theory we expect that the center of the plate deforms approximately in plane strain, while the surface of the plate deforms as in plane stress. There

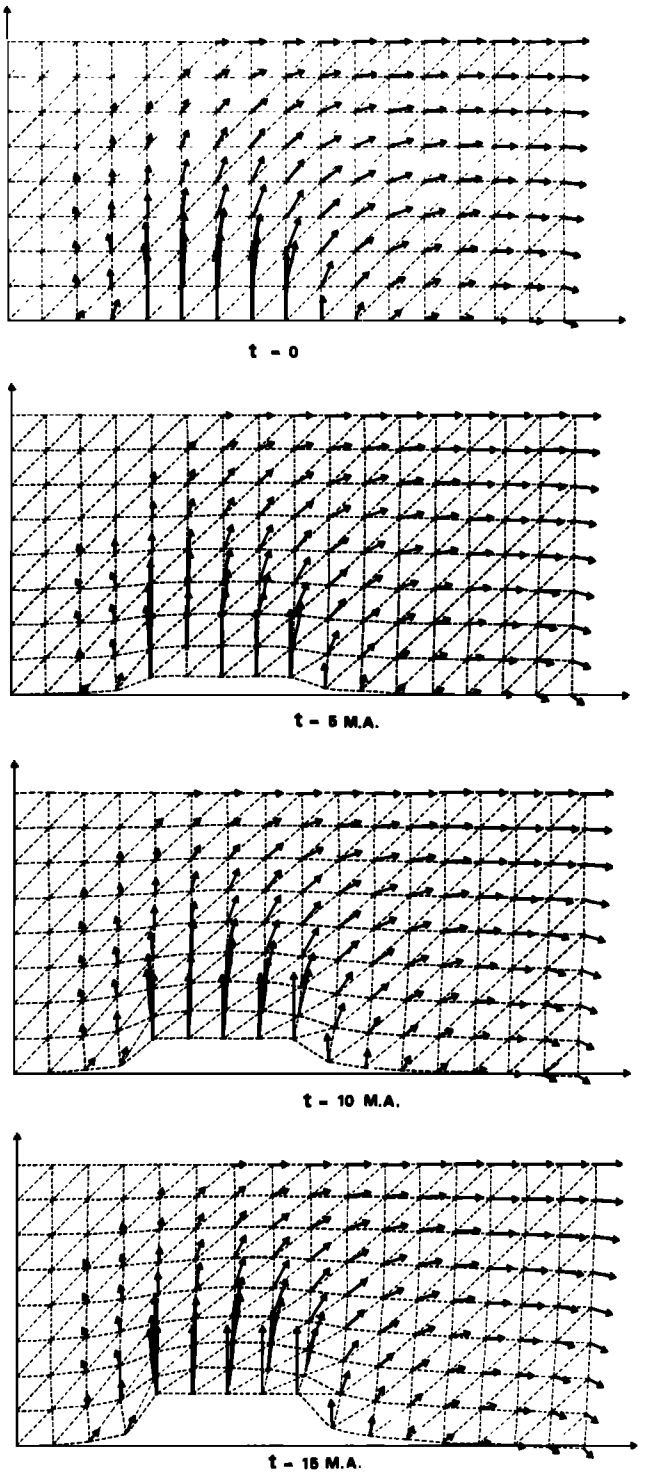

Fig. 14. Horizontal velocity field and deformed grid as a function of time for the asymmetric plane stress model shown at the bottom of Figure 2 with a creep law (n = 3). The vectors indicate instantaneous velocities at the displaced grid points.

should be a complex coupling between the behavior at the center and at the surface of the plate. The average behavior of the lithosphere should be integrated across the thickness of the plate. Such an approach requires three-dimensional solutions which are beyond our possibilities at present.

Our results for plane strain and plane stress in the case of a free lateral wall are not very different, however, for the horizontal motion and deviatoric stresses. This agreement improves as we move away from the indenter. In this case then the two-dimensional solutions obtained here are a good approximation to the deformation of a thick plate. The same is not true for the rigid lateral wall since the plane strain model insures incompressibility by a return flow on the sides of the indenter, while in plane stress this is obtained by thickening or thinning of the plate. In this case then the solution for a thick plate may have to be eventually discussed by three-dimensional models.

We discuss now our results in terms of the observations made on the collision between India and Eurasia. The asymmetry of the stress field to the east and west of the collision front, with a rotation of almost 90° to the west and an S-like rotation to the east, may be related to a difference in the boundary conditions on both sides of the Himalayas (Figure 15). The S-like variation of the orientation of the stress field is observed in our results both for plane stress and plane strain, but only for free boundary conditions to the E of the plate. The S-like stress field may be explained if the eastern boundary, at the Pacific subduction zone, is approximately stress free. To the west, the rotation of the stress field may be explained by our models if we adopt a rigid boundary condition. This may be associated with an artificial boundary separating the region of large deformation from another to the west where the strain rate is negligible.

The plane strain results show very large values of the vertical stress σ_{zz} in front of the indenter. This is due to the tendency of the material to deform vertically; a large vertical pressure is required to force the deformation to be restricted to a plane, as assumed in plane strain. This explains why the plane stress mode is important: in order to maintain plane incompressible strain, large vertical stresses averaged over the lithosphere have to be accepted. These stresses are of the order of several hundred bars to a few kilobars, according to our results.

Our plane stress results seem in good agreement with certain aspects of the observed faulting pattern in Asia if we make the hypothesis that the faulting in the surface brittle layer reflects the state of stress at the deeper flowing layer. We observe a zone compatible with thrust faulting ahead of the indenter, while farther away, to the sides of the punch, the maximum and minimum principal stresses are horizontal, the condition for strike slip faulting. We also note extensional stresses, the condition for normal faulting, near the free lateral walls. This may be correlated with the normal faulting observed in Yunnan and Shansi, the size of the normal fault areas depending on the exponent of the creep law. We note that these results were obtained without consideration of gravity, which should most likely emphasize even more these features, so that they are clearly related to the indentation. Let us remark also that this extension is associated with a thinning of the lithosphere, which also agrees

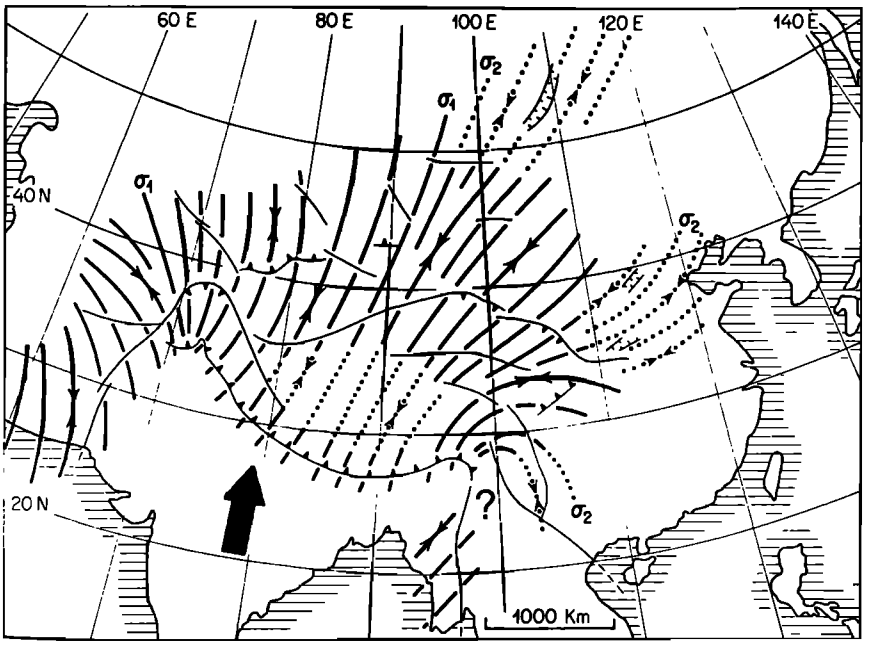

Fig. 15. Maximal horizontal stress direction in Asia infered by Mattauer and Mercier (1980) from geological observations. Note the S-like rotation of the stress direction to the east of Tibet.

with observations at Yunnan and Shansi. However, we never found any results that could evoke the Baikal extensional structure, which seems to involve a more complicated mechanism. In all our plane stress results we find that the vertical motions are small when compared to the horizontal strains, which is entirely compatible with observations. Yhe small vertical motions alone may not be invoked to justify the use of a plane strain approximation.

Tapponnier and Molnar (1976) and Tapponnier (1978) suggested that the arcs to the side of the Himalayas were due to the material movement toward the free boundaries as a consequence of the indentation. This return movement is present in incompressible plane strain only if the lateral wall is rigid, i.e., if the matter may not escape through the lateral walls. As shown in Figure 6, this return motion does not exist in plane stress since the material moves preferably in the vertical direction, thickening or thinning the plate.

In front of the indenter, for plane stress we observe a significant zone of plate thickening which we may associate with the Tibetan plateau. Our results show that its extents toward the interior of the plate and on the sides of the indenter are controlled by the exponent of the creep law: the higher the nonlinearity of the law, the sharper are the boundaries of the elevated zone. Our plane stress results do not show, however, a lateral extension regime in front of the punch that we could associate with the normal faulting in Tibet observed by Chen and Molnar (1981), Ni and York (1978), and Tapponnier et al. (1981). It is possible that this normal faulting may be due to the lateral push induced by gravity on the elevated areas. We have not yet incorporated the effect of gravity in our plane stress calculation (gravity would have no effect in plane strain, since there is no vertical motion in this case) but it will be the subject of further research.

There are no topographic peaks at the eastern edges of the Himalaya range which could be related to the vertical strain rate concentrations near the edges of the punch, as shown on Figures 11, 12, and 13. However, the outcrops of the deeper crustal rocks at both ends of the Himalayan range may be due to the erosion of crustal layers that have been uplifting more rapidly near the end zones than elsewhere in the Himalayas. Thus the vertical strain rate concentrations exist, but they are continuously rounded down by erosion.

Conclusions

We have presented two finite element methods for the study of two-dimensional viscoplastic flow. One of these methods, based on a weighted residuals approach is found to be more efficient in the solution of plane strain problems. The other method, based on the minimization of a convex functional, is more efficient in plane stress problems. With these two methods we solved the problem of indentation of a rectangular plate by a rigid die penetrating at constant velocity. Plane strain and plane stress solutions were studied for a number of choices of boundary conditions and rheological laws. We find that the boundary conditions on lateral walls far from the indenter have very large effects on the characteristics of the plastic flow. For a free lateral wall the flow is preferentially in the lateral direction, as had been proposed by Tapponnier and Molnar (1977), while for a rigid lateral wall the flow pattern differs according to the mode of deformation. For plane stress (thin plate model) the plate thickens or thins in the vertical direction, while for plane strain (very thick plate model) there is a large return flow on the sides of the indenter. The actual condition for the lithosphere, a mode-

rately thick plate, should be intermediate between these two extreme models.

A nonlinear creep rheology was adopted, and it is shown that the main effect of increasing the exponent of the power law is to sharpen the flow features, concentrating the differential motion on rather narrow bands. The effect of a finite creep strength or yield stress is similar.

Finally, the stress patterns and the vertical motions are compared to some observations made on the Indian-Asian collision.

Appendix A: Weighted Residuals Method

Let Ω be the domain under study, with a boundary Γ (of normal $\underline{n}$) which may be decomposed into Γ_v, where velocity is specified, and Γ_τ, where stress is given. In Ω a body force density $\underline{f}$ is specified. Including the condition of incompressibility for the flow our problem consists in the determination of the velocity field $\underline{u}$ and the stress field $\underline{\underline{\sigma}}$ that satisfy the following system

$$\sigma_{ij,j} + f_i = 0 \qquad \text{in } \Omega \tag{A1}$$

$$u_{i,i} = 0 \qquad \text{in } \Omega \tag{A2}$$

$$u_i = \tilde{v}_i \qquad \text{on } \Gamma_v \tag{A3}$$

$$\sigma_{ij} n_j = \tau_i \qquad \text{on } \Gamma_\tau \tag{A4}$$

to which we add the constitutive relation

$$\sigma_{ij} = -p\delta_{ij} + \mu(u_{i,j} + u_{j,i}) \tag{A5}$$

where μ is the nonlinear equivalent viscosity defined by (9).

In order to solve the problem with stress and velocity as the variables, we adopt a penalty function method [Zienkiewicz, 1977; Hughes et al., 1979]. This allows replacement of problem (A1) to (A4) by an associated problem where the incompressibility (A2) is insured by means of a penalty function [Oden, 1978]. Let us define the Sobolev space $H_1(\Omega)$ of functions defined on Ω such that they and their first-order partial derivatives are square integrable. The problem is to find a function $\underline{u}(\varepsilon)$ (and $\underline{\underline{\sigma}}(\varepsilon)$) such that

$$\begin{aligned}
&\sigma_{ij,j}(\varepsilon) + f_i = 0 && \text{in } \Omega \\
&u_i(\varepsilon) = \tilde{v}_i && \text{on } \Gamma_v \\
&\sigma_{ij}(\varepsilon) n_j = \tau_i && \text{on } \Gamma_\tau \\
&\sigma_{ij}(\varepsilon) = -p(\varepsilon)\delta_{ij} + \mu(u_{i,j} + u_{j,i}) \\
&-p(\varepsilon) = -\psi(\varepsilon)\, \nabla\cdot\underline{u}(\varepsilon) + p_0
\end{aligned} \tag{A6}$$

where p_0 is a constant, and $\psi(\varepsilon)$, the penalty function, has the property that for every $0 < \varepsilon < 1$, there exists a ψ_0 such that

$$0 < \psi_0 < \psi(\varepsilon) < \infty \tag{A7}$$

It is possible to show that (A6) admits a solution for every value of ε and that if $\lim \varepsilon \to 0\ \psi(\varepsilon) = \infty$, the solution $\underline{u}(\varepsilon)$ converges toward the solution of the problem (A1) to (A4) [Reddy, 1978]. In our calculations we have adopted $\psi(\varepsilon) = 1/\varepsilon$.

The problem (A6) once μ is replaced by the expression (9), is posed in terms of velocities only. We look for velocities of the form

$$\underline{u}(\varepsilon) = \underline{w}(\varepsilon) + \underline{v}(\varepsilon) \tag{A8}$$

where

$$\begin{aligned}
&\underline{w} \in H_1(\Omega) \quad \text{and} \quad \underline{w} = \underline{0} \quad \text{on } \Gamma_v \\
&\text{and} \\
&\underline{v} \in H_1(\Omega) \quad \text{and} \quad \underline{v} = \tilde{\underline{v}} \quad \text{on } \Gamma_v
\end{aligned} \tag{A9}$$

In the finite element method we discretize the domain Ω into a set $\bar{\Omega}$ of elements Ω^e characterized by a grid parameter $0 < h < 1$. We find in this way the best approximation $\underline{u}^h(\varepsilon)$ to $\underline{u}$ in a subset $H_1^h(\Omega)$ of $H_1(\Omega)$. We replace $\underline{u}(\underline{x})$ defined in Ω by a function $\underline{u}^h(\varepsilon)$ defined at the nodal points of the discrete approximation $\bar{\Omega}$. We restrict $\underline{u}^h(\varepsilon)$ to the element Ω^e, which we have chosen to be of the 8-node isoparametric serendipity type. Then, omitting h and ε for notation simplicity,

$$\underline{u}^e(\underline{x}) = \sum_{i=1}^{N} \phi_i^e(\underline{x})\, \underline{u}(\underline{x}_i^e) \tag{A10}$$

where $\underline{x}_i^e$ is the position of the ith node of the eth element. The shape functions have the properties

$$\begin{aligned}
&\phi_i^e(\underline{x}_j^{e'}) = 0 \quad \text{if } \underline{x}_j^{e'} \notin \Omega^e \\
&\phi_i^e(\underline{x}_j^e) = \delta_{ij} \quad \text{if } \underline{x}_j^e \in \Omega^e
\end{aligned} \tag{A11}$$

The form functions $\phi_i^e(\underline{x})$ for the 8-node serendipity element are from Zienkiewicz [1977, p. 174]. The problem may now be reduced to finding $\underline{w}$ and $\underline{v}$ in $H_1(\Omega)$, such that

$$P(\underline{w} + \underline{v}) = \underline{f} \tag{A12}$$

where P is a nonlinear operator. Restricting P to functions defined only on Ω_e and denoting it P_e, we define the residue

$$r_e(\underline{x}) = P_e(\underline{w}^e + \underline{v}^e) - f^e \tag{A13}$$

and the goal is to find the functions $\underline{w}^e$ and $\underline{v}^e$ that minimize this residue. For this purpose we adopt a weighted residual method. We introduce the weighting function $\omega^e(\underline{x})$ defined on the element e and require that the residue averaged on the element be zero:

$$\int_{\Omega^e} r^e(\underline{x})\, \omega^e(\underline{x})\, d\Omega_e = 0 \tag{A14}$$

We shall use here Galerkin's version of the weighted residual method. In this case the weighting functions ω are expanded with the same shape functions used for the expansion of velocity (see (A10)):

$$\underline{\omega}^e(\underline{x}) = \sum_{i=1}^{N} \phi_i^e(\underline{x})\, a_i^e \tag{A15}$$

with $\underline{\omega}^e(\underline{x}_i^e) = a_i^e$.

Instead of using (A14) directly we have adopted a weaker version of it from Hughes et al. [1979], which we write

$$\int_\Omega (\psi(\varepsilon)\nabla\cdot\underline{w}\ \nabla\cdot\underline{\omega} + 2\mu(\nabla\underline{w}):(\nabla\underline{\omega}))\ d\Omega = \int_\Omega \underline{f}\cdot\underline{\omega}\ d\Omega \quad (A16)$$
$$+ \int_{\Gamma_\tau} \underline{\tau}\cdot\underline{\omega}\ d\Gamma - \int_\Omega (\psi(\varepsilon)(\nabla\cdot\underline{v})(\nabla\cdot\underline{\omega}) + 2\mu(\nabla\underline{v}):(\nabla\underline{\omega}))d\Omega$$

Substituting the weights $\underline{\omega}$ and velocities $\underline{v}$, $\underline{w}$ by their expansions (A15),(A10) in terms of the basis function $\phi_i^e(\underline{x})$ we obtain the matrix equation of the finite element method from the requirement that (A16) be satisfied for arbitrary a_i^e:

$$\underline{\underline{K}}\ \underline{W} = \underline{F} \quad (A17)$$

where the rigidity matrix is assembled from the elementary matrices defined explicitely by

$$\underline{\underline{K}}^e = \begin{bmatrix} \mu(2\underline{\underline{K}}^{11}+\underline{\underline{K}}^{22})+\psi(\varepsilon)\underline{\underline{K}}^{11} & \psi(\varepsilon)\underline{\underline{K}}^{12}+\mu(\underline{\underline{K}}^{12})^T \\ \psi(\varepsilon)\underline{\underline{K}}^{12}+\mu(\underline{\underline{K}}^{12})^T & \mu(\underline{\underline{K}}^{11}+2\underline{\underline{K}}^{22})+\psi(\varepsilon)\underline{\underline{K}}^{22} \end{bmatrix} \quad (A18)$$

where the component matrices $\underline{\underline{K}}^{1k}$ are defined by

$$K_{ij}^{1k} = \int_{\Omega^e} (\partial\phi_i/\partial x_1)(\partial\phi_j/\partial x_k)\ d\Omega^e$$

The pressure $p(\varepsilon)$ may be calculated accessorily by

$$p(\varepsilon) = -\psi(\varepsilon)\nabla\cdot\underline{u}(\varepsilon)$$

The force vector $\underline{F}$ in (A17) is also assembled from the elementary force vectors for every element [Zienkiewicz, 1977], and the vector $\underline{W}$ is the solution vector assembled from the nodal velocities $\underline{v}(x_i^e)$ and $\underline{w}(x_i^e)$.

The system of equations (A17) was solved by a frontal method adapted to the modified Newton iterative algorithm [Irons and Ahmad, 1980]. The stresses and strains were calculated at the points of numerical integration in order to improve their estimation. The precision of the iterative solution depends on the way ε approaches zero. There appear certain stability problems that we solved by the use of a collective reduced Gauss integration (2 x 2) in the calculation of the rigidity matrix $\underline{\underline{K}}$ of (A18). Sani et al. [1982] showed that for $c < \mu\varepsilon < 1$ the solutions are stable if c is the truncation error of the computer being used. Unfortunately, the numerical solution may still present spurious or hour glass modes that depend on the boundary conditions that have been adopted. We have carefully checked that this problem is not present in our solutions.

Appendix B : The Flow of a Nonlinear Creeping Material

We present here the method that we use to generate solutions for the plane stress case. The method is from Friaa [1979] and Delbecq et al. [1977] and is applicable only to nonlinear creep without flow limit (i.e., $\sigma_y = 0$). In this case we may rewrite the flow law (13), introducing a potential

$$\phi(\dot{\underline{\underline{\varepsilon}}}) = n/(n+1)\ \alpha^{-1/n}\ (\sqrt{I_2})^{(n+1)/n} \quad (B1)$$

so that

$$\sigma_{ij} = \partial\phi(\dot{\underline{\underline{\varepsilon}}})/\partial\dot{\varepsilon}_{ij} \quad (B2)$$

It may be shown that during the flow the solution for the velocity field has to satisfy the following conditions: (1) it minimizes the functional

$$H(\underline{u}) = \int_\Omega \phi(\dot{\underline{\underline{\varepsilon}}})\ d\Omega - \int_{\Gamma_\tau} \underline{\tau}\cdot\underline{u}\ d\Gamma - \int_\Omega \underline{f}\cdot\underline{u}\ d\Omega \quad (B3)$$

and (2) it is kinematically admissible, i.e., it is incompressible ($\nabla\cdot\underline{u} = 0$) and satisfies the velocity boundary conditions on Γ_v. The finite element approximation to this problem consists in finding the best approximation to $\underline{u}$ in a discrete approximation of the space Ω. In the computer implementation used here, we choose 3-node triangular elements. Introducing the notation $p = (n+1)/n$, we reduce the problem to the minimization of

$$\sum_{e=1}^{N} 1/p \int_{\Omega^e} (\underline{u_e}^T\ \underline{\underline{A}}_e\ \underline{u_e})^{p/2} d\Omega^e - \underline{W}^T\underline{F} \quad (B4)$$

where $\underline{u_e}$ is the vector of nodal velocities that we decompose in two parts $\underline{u_e} = \underline{w} + \underline{v}$ with $\underline{w}$ incompressible, i.e., $\nabla\cdot\underline{w} = 0$. $\underline{v}$ is a vector whose only nonzero components are the velocities of the nodes where a velocity boundary condition is imposed. In the vector $\underline{w}$ the velocities of the nodes where a velocity is imposed are put to zero. Finally, $\underline{\underline{A}}_e$ is the rigidity matrix for the element e.

The incompressibility is insured by a saddle point method:

$$\underset{\underline{\Lambda}}{\mathrm{Sup}}\ \left(\underset{\underline{u}}{\mathrm{Inf}}\ \left(\sum_{e=1}^{N} 1/p \int_{\Omega^e} (\underline{u_e}^T\ \underline{\underline{A}}_e\ \underline{u_e})^{1/p}\ d\Omega^e + \int_{\Omega^e} \underline{\Lambda}^T\ \underline{\underline{D}}_e\ \underline{w_e}\ d\Omega^e - \underline{W}^T\underline{F}\right)\right)$$

where $\underline{\underline{D}}_e$ is the incompressibility matrix for the element e and $\underline{\Lambda}^T$ is a Legendre coefficient vector. This problem is solved by a variation of Uzawa's method developped by Delbecq et al. [1977].

For the plane stress problem, the incompressibility on the plane is not necessary (see (19)) and we only have to minimize (B4). This is achieved by a gradient method. A more detailed description of the method may be found from Friaa [1979].

Acknowledgments. One of us (M.D.) wishes to thank Michel Fremond, Ahmed Friaa, and the Laboratoire Central des Ponts et Chaussées (Department Mathématiques) for their assistance in the second finite element method of this work. Acknowledgment of the authors is also extended to Paul Tapponnier, Dan P. McKenzie, and P. England for a number of interesting discussions. This work has been supported by the Institut National d'Astronomie et de Géophysique as a part of its geodynamic program (A.T.P. Géodynamique, contract 3375).

References

Argand, E., La tectonique de l'Asie, Int. Geol. Congr. Rep. Sess. 13, I(5),171-322, 1924.

Ashby, M. F., and R. A. Verrall, Micromechanisms of flow and fracture, and their relevance to the rheology of the upper mantle, Philos. Trans. R. Soc. London, Ser A., 288, 59-95, 1977.

Backoffen, W. A., Deformation Processing, Addison-Wesley, Reading, Mass., 1972.

Bird, P., Finite elements modeling of lithosphere deformation: The Zagros collision orogeny, Tectonophysics, 50, 307-336, 1978.
Bird, P., and K. Piper, Plane stress finite element models of tectonic flow in southern California, Phys. Earth Planet. Inter., 21, 158-175, 1980
Bird, P., and M. N. Toksöz, Strong attenuation of Rayleigh waves in Tibet, Nature, 266, 161-163, 1977.
Brace, W. F., and D. L. Kohlstedt, Limits on the lithospheric stress imposed by laboratory experiments, J. Geophys. Res., 85, 6248-6252, 1980.
Byerlee, J., Friction in rocks, Pure Appl. Geophys., 116, 615-626, 1978.
Carter, N. L., and H. G. Ave'Lallemant, High temperature flow in dunite and peridotite, Geol. Soc. Am. Bull., 81, 2181-2202, 1970.
Cathles, L. M., III, Viscosity of the Earth's Mantle, Princeton University Press, Princeton, N. J., 1975.
Chen, W. P., and P. Molnar, Constraints on the seismic wave velocity structure beneath the Tibetan plateau and their tectonic implications, J. Geophys. Res., 86, 5937-5962, 1981.
Daignières, M., M. Fremond, and A. Friaa, Modèle de type Norton-Hoff généralisé pour l'étude des déformations lithosphériques (exemple: la collision Himalayenne), C.R. Hebd. Séances Acad. Sci., 268B, 371-374, 1978.
Delbecq, J. M., M. Fremond, A. Pecker, and J. Salençon, Elements finis en plasticité et en viscoplasticité, J. Méc. Appl., 1, 267-304, 1977.
Friaa, A., La loi de Norton-Hoff généralisée en plasticité et viscoplasticité, thèse doctorat d'Etat, Univ. Paris, 1979.
Goetze, C., The mechanism of creep in olivine, Philos. Trans. R. Soc. London, Ser. A., 288, 99-119, 1978.
Hill, R., The Mathematical Theory of Plasticity, Oxford University Press, New York, 1950.
Hughes, T. J. R., W. K. Liu, and A. Brooks, Finite element analysis of incompressible viscous flows by the penalty function formulation, J. Comp. Phys., 30, 1-60, 1979.
Irons, B., and S. Ahmad, Techniques of Finite Elements, Ellis Horwood, Chichester, 1980.
Jeffreys, H., The Earth, Cambridge University Press, New York, 1976.
Kirby, S. H., Tectonic stresses in the lithosphere constraints provided by the experimental deformation of rocks, J. Geophys. Res., 85, 6353-6363, 1980.
Mandel, J., Plasticité Classique et Viscoplasticité, cours C.I.S.M., Udine, Springer-Verlag, New York, 1972.
Mattauer, M., and J. L. Mercier, Microtectonique et grande tectonique, Mém. hors Sér. Soc. Géol. Fr., 10, 141-161, 1980.
McNutt, M., Implication of regional gravity for state of stress in the earth's crust and upper mantle, J. Geophys. Res., 85, 6377-6396, 1980.
Melosh, H. J., and A. Raefsky, The dynamical origin of subduction zone topography, Geophys. J. R. Astron. Soc., 60, 333-354, 1980.
Molnar, P., and P. Tapponnier, Cenozoic tectonics of Asia: Effects of a continental collision, Science, 189, 419-426, 1975.
Molnar, P., and P. Tapponnier, Cenozoic tectonics of Tibet, J. Geophys. Res., 83, 5361-5375, 1978.
Neugebauer, H. J., M. Wallner, and D. L. Turcotte, Aspects of lithospheric collision - Numerical experiments (abstract), Eos Trans. AGU, 62, 812, 1981.
Ni, J., and J.E. York, Late Cenozoic extensional tectonic of the Tibetan plateau, J. Geophys. Res., 83, 5377-5387, 1978.
Oden, J. T., A theory of penalty method for finite element approximation of highly non linear problems in continuum mechanics, Comp. Struct., 8, 445-449, 1978.
Perzyna, P., Fundamental problems in viscoplasticity, Adv. Appl. Mech., 09, 243-377, 1966.
Post, R.L., Jr., High temperature creep of Mt. Burnett dunite, Tectonophysics, 42, 75-110, 1977.
Reddy, J. N., On the accuracy and existence of solutions to primitive variable models of viscous incompressible fluids, Int. J. Eng. Sci., 16, 921-929, 1978.
Sani, R. L., M. P. Gresho, R. L. Lee, D. F. Griffiths, and M. Engelman, The cause and cure (?) of the spurious pressures generated by certain F.E.M. solutions of incompressible Navier-Stockes equations; parts I and II, Int. J. Numer. Method. Fluids, 1, in press, 1982.
Tapponnier, P., Les mécanismes de la déformation intracontinentale: Exemple de la tectonique alpine en Asie et en Europe, thèse de doctorat d'Etat, Univ. Montpellier, 1978.
Tapponnier, P., and P. Molnar, Slip line field theory and large-scale continental tectonics, Nature, 264, 319-324, 1976.
Tapponnier, P., and P. Molnar, Active faulting and tectonics in China, J. Geophys. Res., 82, 2905-2930, 1977.
Tapponnier, P., J. L. Mercier, R. Armijo, H. Tonglin, and Z. Ji, Field evidence for active normal faulting in Tibet, Nature, 294, 410-414, 1981.
Vilotte, J. P., Quelques essais d'approches numériques et mécaniques de la déformation. Exemple: Le poinçonnement plan, diplôme d'Etudes Approfondies, Univ. Montpellier, 1980.
Vilotte, J. P., and M. Daignières, A numerical approach for some cases of mean continental deformation (abstract), Eos Trans. AGU, 62, 812, 1981.
Weertman, J., Creep laws for the mantle of the earth, Philos. Trans. R. Soc. London, Ser.A., 288, 9-26, 1978.
Weertman, J., and J. R. Weertman, High temperature creep of rock and mantle viscosity, Annu. Rev. Earth Planet. Sci., 3, 293-315, 1975.
Zarka, J., Généralisation de la théorie du potentiel plastique multiple en viscoplasticité, J. Mech. Phys. Solids, 20, 179-195, 1972
Zienkiewicz, D. C., The Finite Element Method, McGraw-Hill, New York, 1977.
Zienkiewicz, D. C., and P. N. Godbole, A penalty function approach to the surface deformation, J. Strain. Anal., 10, 180-185, 1975.
Zienkiewicz, D. C., P. C. Jain and E. Onate, Flow of solids during forming and extrusion: some aspects of numerical solutions, Int. J. Solids Struct., 14, 15-38, 1978

(Received February 4, 1982;
revised June 4, 1982;
accepted June 11, 1982.)